

---

# Explaining and Adapting Graph Conditional Shift

---

Qi Zhu\*   Yizhu Jiao\*   Natalia Ponomareva†   Jiawei Han\*   Bryan Perozzi†

\*: University of Illinois Urbana-Champaign †: Google Research  
\*{qiz3,yizhu2,hanj}@illinois.edu,  
†{nponomareva,bperozzi}@google.com

## Abstract

Graph Neural Networks (GNNs) have shown remarkable performance on graph-structured data. However, recent empirical studies suggest that GNNs are very susceptible to distribution shift. There is still significant ambiguity about *why* graph-based models seem more vulnerable to these shifts. In this work we provide a thorough theoretical analysis on it by quantifying the magnitude of *conditional shift*<sup>1</sup> between the input features and the output label. Our findings show that both graph heterophily and model architecture exacerbate conditional shifts, leading to performance degradation. To address this, we propose an approach that involves estimating and minimizing the conditional shift for unsupervised domain adaptation on graphs. In our controlled synthetic experiments, our algorithm demonstrates robustness towards distribution shift, resulting in up to 10% absolute ROC AUC improvement versus the second-best algorithm. Furthermore, comprehensive experiments on both node classification and graph classification show its robust performance under various distribution shifts.

## 1 Introduction

Graph Neural Networks (GNNs) [19, 33, 17, 10] are powerful tools that have showed excellent performance on graph structured data. Interestingly, recent work has revealed that GNNs shows a susceptibility to performance degradation when confronted with data distribution shift, where the data used for training (*source data*) and inference (*target data*) come from different distributions [21, 39]. Consequently, there has been a growing interest in investigating the behavior of GNNs under distribution shift, which demonstrate that both shifts in graph structure and node features can lead to a deterioration in GNN performance [46, 26, 34]. However, these works are primarily empirical, and there are still many open questions about both the nature of this susceptibility, as well as how to address it effectively.

At the same time, extensive research has been conducted to examine the behavior of conventional machine learning models (excluding GNNs) in the presence of domain shift. Two prominent settings that have received significant attention are Unsupervised Domain Adaptation (UDA) and Domain Generalization (DG). When unlabeled target data is available, common UDA approaches including learning Domain Invariant Representation Learning (DIRL) [5, 14] attempts to align latent representations of source and target data. Another approach, Domain Generalization (DG) [1], addresses the challenge of training models that can generalize effectively to unseen target domains by leveraging multiple source domains during training.

---

<sup>1</sup>Conditional shift represents a change in the conditional distribution  $\mathbf{P}(y|x)$  between the input features  $x$  and the corresponding output labels  $y$  when moving from the source domain to the target domain.

In this paper, our focus is on node classification [19], a fundamental task in GNNs, where the effectiveness of DIRM methods [14] has been found to be limited [46]. To address this limitation, we begin with investigating the underlying distribution of latent representations generated by GNNs. Remarkably, we discover that GNNs can exacerbate the conditional shift ( $\mathbf{P}_s(\mathbf{y}|\mathbf{h}) \neq \mathbf{P}_t(\mathbf{y}|\mathbf{h})$ ), thereby challenging the validity of “no conditional shift” assumption ( $\mathbf{P}_s(\mathbf{y}|\mathbf{h}) \approx \mathbf{P}_t(\mathbf{y}|\mathbf{h})$ ) in DIRM methods. In Section 3.2, we provide a thorough theoretical analysis by quantifying the magnitude of conditional shift. Through our investigation into various graph characteristics, we observe that both graph heterophily [45] and model architecture (specifically, graph convolutions [19]) exacerbate conditional shifts. Our theoretical results then show that these shifts provably degrade the generalization capabilities of GNNs. Thus, mitigating the conditional shift is crucial for enhancing unsupervised domain adaptation on graphs.

Inspired by this understanding, we propose a **graph conditional shift adaptation** method, called **GCONDA**, to perform graph UDA. First, we estimate the conditional shift as Wasserstein distance  $\widehat{\mathbf{W}}_1$  between source label distribution  $\mathbf{P}_s(\mathbf{y}|\mathbf{h})$  and estimated pseudo label distribution  $\mathbf{P}_t(\hat{\mathbf{y}}|\mathbf{h})$ . Building upon our theoretical results, we incorporate the calculation and minimization of the estimated conditional shift between the source and unlabeled target batch into the training process. Notably, we enhance our approach by incorporating the distribution discrepancy of the latent representation ( $\mathbf{P}_s(\mathbf{h}), \mathbf{P}_t(\mathbf{h})$ ) into the estimation of  $\widehat{\mathbf{W}}_1$ , which we refer to as **GCONDA++**. In Theorem 4.1, we discuss the generalization bound of GNNs with  $\widehat{\mathbf{W}}_1$  and the Lipschitz constant of GNNs [11, 40].

Specifically, our theoretical and practical contributions are the following:

**(i). Derivation of graph conditional shift and its implications.** Using a CSBM model, we provide the *first provable result* (Theorem 3.1) quantifying how GNNs worsen conditional shift. Subsequent analysis (Corollary 3.1.1) identifies graph heterophily and graph convolutions as two contributing factors to the unsatisfactory performance of GNNs under distribution shifts. This finding (Corollary 3.1.2) further offers insights into the practical implications and applications of GNNs.

**(ii). Graph UDA by minimizing conditional shift.** Building upon our theoretical findings, we propose **GCONDA**, a graph UDA method that leverages the minimization of conditional shift. In practice, we observe a strong correlation between the estimated Wasserstein distance and the actual performance of the GNN model. In contrast, other latent representation distances that do not exhibit the same level of correlation (*e.g.* CMD [41] in Figure 2),

**(iii). Robustness towards different distribution shifts.** On synthetic graphs, **GCONDA** demonstrates a substantial performance advantage over other DIRM baselines, with an absolute AUC\_ROC improvement of up to 10%. In the node classification task, **GCONDA** consistently outperforms competing methods across six real-world datasets, demonstrating superior performance even under various types of shifts. Additionally, when applied to graph classification, our approach leads to performance improvements as well.

## 2 Related Work

**Unsupervised Domain Adaptation.** The goal of UDA algorithms is to transfer knowledge from the source onto target data, obtaining good generalization on target distribution. In the theoretical foundational work of domain adaptation, [5] presented an upper bound of target risk using the performance of the model on source data and introduced a domain discrepancy measure called  $\mathcal{H}$ -divergence. Since then, many domain adaptation algorithms that minimize differences between source and target domains have been proposed [14, 25, 15, 24, 41]. For example, DANN [14] achieves domain invariant learning (DIRL) by introducing an adversarial objective to distinguish source and target samples in the latent space. Conditional DANN work - CDAN [25] - incorporates classifier predictions into the adversarial head, either via linear or multilinear conditioning, further improving UDA performance. Besides, some other work propose to match the distribution in the latent space through probability discrepancy measures like MMD [15, 24] and CMD [41]. In a recent study [44], it was demonstrated that existing methods for UDA suffer from poor generalization when there is variation in the conditional probability  $\mathbf{P}(\mathbf{y}|\mathbf{x})$  across domains. In response to this

challenge, Wasserstein distance on joint [12] or label distribution [23] are proposed to guide the mapping between source and target samples using optimal transport.

**Graph Domain Adaptation.** Graph Representation Learning introduces new out-of-distribution (OOD) challenges based on the graph structure (including graph size [7, 39], molecular scaffolds[16]). The first several studies[43, 34, 9] adopted domain invariant learning across source and target graphs assuming covariate shift. On semi-supervised learning, SRGNN[46] introduced a combination of instance weighting and DIRT techniques to enhance OOD generalization in the presence of localized training data. Other pioneering work tried to capture environment-invariant node properties [35] and substructures [37] guided by reinforcement learning based environment generators. In the meantime, theoretical analysis on the generalization bound of Graph Domain Adaptation (GDA) approaches is advancing. The Tree-mover’s distance [11] provided a model-agnostic generalization bound for GNNs when facing distribution shift. Additionally, the first model-based GDA bound [40] proposed to optimize the Lipschitz constant of GNNs through spectral regularization.

Existing domain adaptation algorithms for GNNs primarily focused on enhancing model design to achieve improved empirical performance. Unlike all these methods, our work introduces a novel perspective - *conditional shift* to explain and mitigate the distribution shift for graph data.

### 3 Understanding Distribution Shift in GNNs

#### 3.1 Background: Graph UDA

**Notations.** A graph is described by a tuple  $\mathcal{G}(V, A, X)$ , where the nodes  $V$  are associated with their features  $X \in \mathbb{R}^{|V| \times d}$  and the adjacency matrix  $A \in \mathbb{R}^{|V| \times |V|}$  describes the connections between nodes. We denote  $Y$ , ( $Y \in \mathbb{Z}^{|V| \times |L|}$ ), as labels for all nodes in graph  $\mathcal{G}$  and  $x_i, y_i$  represent a single node’s features and label ( $y_i \in L$ ). A Graph Neural Network  $g$  stacks several neural network layers which transform nodes and their neighborhood information into a latent representation  $g : (X, A) \rightarrow H$ . Each layer of a GNN can be described by:

$$H^k = \sigma(\tilde{A}H^{k-1}\theta^k), \quad (1)$$

where  $\tilde{A}$  is a transformed adjacency matrix that is defined by a specific GNN method.

The task of node classification takes nodes features  $X$  and structure of the graph  $A$  to predict labels  $Y$  through a GNN encoder  $g$  and classifier  $f$ . Let the embedding  $h_i$  be node  $i$ ’s representation calculated by the final activations of a GNN’s output  $H$ . Then the task of binary node classification predicts the label using classifier  $f$  as follows,

$$f(\mathbf{h}) = \begin{cases} 1, & \text{if } \mathbf{w}^T \mathbf{h} + b > 0 \\ -1, & \text{otherwise} \end{cases} \quad (2)$$

**Graph Unsupervised Domain Adaptation.** Given a source and target graph  $\mathcal{G}_S(V^s, A^s, X^s)$  and  $\mathcal{G}_T(V^t, A^t, X^t)$ , we assume embeddings  $\mathbf{h}^s$  and  $\mathbf{h}^t$  are output by the same GNN. The Unsupervised Domain Adaptation (UDA) algorithm utilizes labeled source  $\{(\mathbf{h}^s, \mathbf{y}^s)\}$  data and unlabeled target data  $\{\mathbf{h}^t\}$ . Let  $\varepsilon$  denote the expected risk of a binary classification problem defined above, then UDA aims to find a predictive classifier  $f$  and GNN  $g$  that achieves small target risk  $\varepsilon_{\mathcal{T}}(f \circ g)$  on  $\mathcal{G}_T$ .

To quantify the discrepancy between source and target distributions  $\mu_S$  and  $\mu_T$ , we mainly use Wasserstein distance in this paper. In addition, we denote  $\mu^f$  as the conditional distribution  $\mathbf{P}(\mathbf{y}|\mathbf{h})$  and  $\mu^g$  as the representation distribution  $\mathbf{P}(\mathbf{h})$ .

**Definition 3.1** (Wasserstein distance). *Wasserstein distance is defined between probability distributions  $\mu_S$  and  $\mu_T$  on metric space  $M$ , using distance function  $d, d : M \times M \rightarrow \mathbb{R}$ ,*

$$\mathbf{W}_p(\mu_S, \mu_T) = \left( \inf_{\gamma \in \Gamma(\mu_S, \mu_T)} \mathbb{E}_{(x,y) \sim \gamma} d(x,y)^p \right)^{1/p}, \quad (3)$$

where  $p$  is the moment of the distance and  $\gamma$  is a joint probability measure on  $M \times M$ .

**Domain-Invariant Representations under Covariate Shift.** Covariate shift refers to a change in the distribution of input features (covariates) between the source and target domains. Although labels

are unavailable for the target data in UDA setting, DURL methods [46, 34] for GNNs instead optimize the following objective, assuming the covariate shift  $\mathbf{P}_s(\mathbf{y}|\mathbf{h}) = \mathbf{P}_t(\mathbf{y}|\mathbf{h})$ ,

$$\min_{f,g} \frac{1}{N} \sum_{i=1}^N \mathcal{L}(y_i^s, h_i^s) + \alpha \mathbf{W}_1(\mu_S^g, \mu_S^g), \quad (4)$$

where  $h_i^s$  is the node representation from GNN’s output  $H$ ,  $\mu_S^g := \mathbf{P}_s(\mathbf{h})$  and  $\mu_T^g := \mathbf{P}_t(\mathbf{h})$  are the marginal distributions of the source and target graphs. The second term minimizes the discrepancy on  $H$ , which is known as learning a domain invariant representation. Besides Wasserstein distance [31], there are several other notable measures used in DURL such as CMD [41] and MMD [24].

Below we give the formal definition of conditional shift.

**Definition 3.2** (Conditional Shift). *Assume  $\mathbf{P}_s(\mathbf{y}|\mathbf{x})$  and  $\mathbf{P}_t(\mathbf{y}|\mathbf{x})$  have the same support on  $\mathbf{x}$ , then conditional shift is defined as  $\Delta_{\mathbf{y}|\mathbf{x}} = \int d(\mathbf{P}_s(\mathbf{y}|x), \mathbf{P}_t(\mathbf{y}|x)) \mathbf{P}_t(x) dx$ ,  $d : L \times L \rightarrow \mathbb{R}^+$ ,  $y \in L$ .*

### 3.2 Conditional Shift in Graph Neural Networks

Now, we present theoretical findings on the occurrence of *conditional shift* in GNNs. Assuming the conditional shift does take place (e.g. covariate shift assumption does not hold), we explore the magnitude of this shift in the input space  $\mathbf{x}$  and latent space  $\mathbf{h}$  of GNNs. To quantify this shift, we use the terms  $\Delta_{\mathbf{y}|\mathbf{h}}$  and  $\Delta_{\mathbf{y}|\mathbf{x}}$  to represent the conditional shift in the latent space and input space, respectively. To analyze the conditional shift on different graph distributions, we use the CSBM [13] graph model, an object of recent interest for understanding GNNs [27, 3].

**Definition 3.3** (Contextual Stochastic Block Model (CSBM)). *The CSBM graph is a tuple  $(A, X, Y)$ , where  $A$  is the node adjacency matrix,  $X$  are the nodes features and  $Y$  are the nodes labels  $\{y_1, \dots, y_n\}$ . These node labels  $y_i$  are random variables drawn from a Bernoulli distribution ( $\text{Ber}(0.5)$ ), and control the connections between nodes in the graph.  $a_{ij} \sim \text{Ber}(p)$  if  $y_i = y_j$  and  $a_{ij} \sim \text{Ber}(q)$  otherwise. Features are drawn according to  $x_i = y_i \mu + \frac{Z_i}{\sqrt{d}}$ ,  $y_i \in \{-1, 1\}$ ,  $\mu \in \mathbb{R}^d$  is the feature mean and  $Z_i \in \mathbb{R}^d$  is a Gaussian random variable.*

The three parameters of CSBM are  $\mu$ ,  $p$ , and  $q$ . They respectively control the closeness of the two classes, the generated graph’s edge density (e.g. average degree  $D$ ) and its homophily ratio<sup>2</sup>. By manipulating  $\mu$  and  $(p, q)$ , it is possible to generate distribution shifts of varying magnitude in both node features and graph structure.

To estimate the conditional shift on target CSBM graph  $\mathcal{G}_T$ , we define  $\Delta_{\mathbf{y}|\mathbf{x}}$  as,

$$\Delta_{\mathbf{y}|\mathbf{x}} = \mathbb{E}_{\mathbf{x} \sim \mathbf{P}_t(\mathbf{x})} \left( \mathbb{I} \left[ \arg \max_y \mathbf{P}_s(\mathbf{y}|\mathbf{x}) \neq \arg \max_y \mathbf{P}_t(\mathbf{y}|\mathbf{x}) \right] \right), \quad (5)$$

**Setting:** The goal of this analysis is to investigate the conditions under which GNNs alleviate such shifts (making covariate shift more likely to hold), or exacerbate them. Here, we use a 1-layer Graph Convolutional Network[19] as our GNN encoder  $g^3$ . On a CSBM graph  $(\mu, p, q)$ , the means of the two classes in the input space are  $(-\mu, \mu)$ , while in the latent space they are  $(-\frac{p-q}{p+q}\mu, \frac{p-q}{p+q}\mu)$ . Without loss of generality, we assume the distribution shift on feature  $\mu$  in  $\mathcal{G}_T$  is controlled by  $\delta \in [0, 1]$ , which moves centroids of both classes in the same direction, that is,  $(-(1 + \delta)\mu, (1 - \delta)\mu)$ .

In Figure 1, we illustrate how shifts in graph structure and node features can result in conditional shift. When the density or homophily ratio ( $D', p'/q'$ ) changes, the class centroid shifts to different positions, as depicted by  $\sqrt{D} \frac{p-q}{p+q} \mu \rightarrow \sqrt{D'} \frac{p'-q'}{p'+q'} \mu$  in Figure 1a. Similarly, if the Gaussian mean moves towards a different position (e.g.  $\mu \rightarrow \mu'$  in Figure 1b), it also contributes to the conditional shift. We begin by deriving the conditional shift and expected error in the following theorem:

**Theorem 3.1** (Conditional Shift in GNNs). *Let the source graph  $\mathcal{G}_S = \text{CSBM}(\mu, p, q)$ , and a target graph  $\mathcal{G}_T = \text{CSBM}(\mu', p', q')$ , where  $D$  and  $D'$  represent their average degrees respectively.*

<sup>2</sup>Homophily ratio calculates the fraction of edges in a graph which connects the nodes that have the same label [45].

<sup>3</sup>While we present here the results for one-layer GCNs and linear perceptron, our results can be extended to multi-layer graph convolutions with activations in the manner of [4]. We leave this for future work.

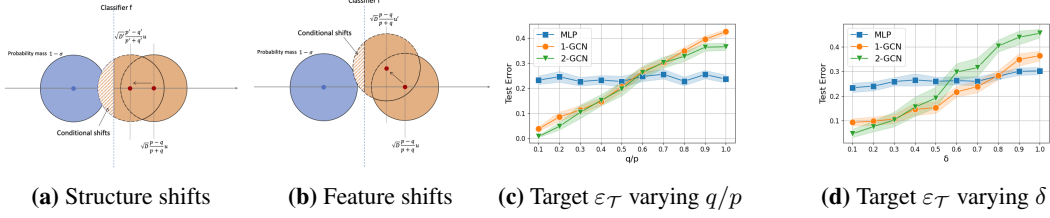


**Figure 1:** Illustration of the conditional shift in a toy 2D latent space. The red points represent the Gaussian means in the latent space. The x-axis represents the direction of feature means ( $\mu$ ), and the conditional shifts are indicated by the area with hatching lines, as defined in Eq. 5. The corresponding generalization results for both shifts are shown in (c) and (d).

Additionally, let  $\Phi(\cdot)$  denote the cumulative distribution function (CDF) of a multivariate Gaussian distribution defined by distance. Then the introduced distribution shift between  $\mathcal{G}_S$  and  $\mathcal{G}_T$  can be quantified via the estimated conditional shift of  $\mathbf{x}$  and  $\mathbf{h}$  as:

$$\Delta_{\mathbf{y}|\mathbf{x}} = \frac{\Phi((1+\delta)\|\mu\|) - \Phi((1-\delta)\|\mu\|)}{2}, \Delta_{\mathbf{y}|\mathbf{h}} = \frac{\Phi(\|\mu'_{h,-1}\|) - \Phi(\|\mu'_{h,1}\|)}{2}, \quad (6)$$

where  $\mu'_{h,1} = \sqrt{D'} \frac{p'-q'}{p'+q'} \mu - \sqrt{D'} \delta \mu$  and  $\mu'_{h,-1} = \sqrt{D'} \frac{q'-p'}{p'+q'} \mu - \sqrt{D'} \delta \mu$ .

*Proof.* See Appendix §A.1. In the proof, we scale the GCN output of the target graph  $\mathbf{h}'$  into a standard Gaussian distribution. Then we can compute  $\Delta$  by comparing the relative position of the optimal classification hyperplane and mean of the Gaussian.  $\square$

Supposing two graphs  $G_1(\mu, p_1, q_1), G_2(\mu, p_2, q_2)$  have the same feature distribution and edge density,  $G_1$  is more heterophilous if it has more edges connecting nodes of different classes, that is  $p_1 < p_2, q_1 > q_2$ . Upon examining the magnitude of the conditional shift  $\Delta_{\mathbf{y}|\mathbf{h}}$  in the two graphs, we find that  $\mu'_{h,-1}(G_1) > \mu'_{h,-1}(G_2)$  and  $\mu'_{h,1}(G_1) < \mu'_{h,1}(G_2)$ . This inequality arises due to the fact that  $\frac{p_1 - q_1}{p_1 + q_1} < \frac{p_2 - q_2}{p_2 + q_2}$ . In other words, Eq. (6) shows that **heterophilous graphs demonstrates a greater degree of conditional shift!**

**Corollary 3.1.1** (GNNs exacerbate Conditional Shift). *Assuming only homophily ratio changes  $p/q \neq p'/q'$ , the conditional shift is always exacerbated by the 1-layer GCN since  $\Delta_{\mathbf{y}|\mathbf{x}} = 0$ . When there is only a feature shift  $\delta\mu$ , the shift will be amplified by the GCN as  $\sqrt{D'}\delta\mu$ , potentially leading to larger conditional shifts.*

Here,  $\Delta_{\mathbf{y}|\mathbf{x}}$  is the conditional shift of a non-graph model (e.g. a multilayer perceptron) and  $\Delta_{\mathbf{y}|\mathbf{h}}$  is the conditional shift of a GCN. Interestingly, Eq. (6) shows GCNs introduce a factor of  $\sqrt{D'}$ , where  $D' > 1$  for any connected graphs. In other words, **GNNs amplify feature shift** (by  $\sqrt{D'}$ ).

**Corollary 3.1.2** (Relation between conditional shift and generalization). *Conditional shift upper bounds the performance gap between source and target, i.e.  $\Delta > |\varepsilon_T - \varepsilon_S|$ . The expected target error  $\varepsilon_T$  for linear classifiers  $f$  and GNNs  $f \circ g$  in section 3.1 are,*

$$\varepsilon_T(f) = 1 - \frac{\Phi((1+\delta)\|\mu\|) + \Phi((1-\delta)\|\mu\|)}{2}, \varepsilon_T(f \circ g) = 1 - \frac{\Phi(\|\mu'_{h,-1}\|) + \Phi(\|\mu'_{h,1}\|)}{2}. \quad (7)$$

Together with the Corollary 3.1.1, we aim to validate the correlation between conditional shift and target error  $\varepsilon_T$ . Therefore, we trained an MLP, a 1-layer GCN, and a 2-layer GCN on a source CSBM graph where GNNs achieves smaller ( $\varepsilon_S \approx 0$ ) than MLP ( $\varepsilon_S \approx 0.2$ ). During testing, we kept the graph density unchanged (i.e.,  $D = D'$ ), while increasing the heterophily ratio  $q'/p'$  or the deviation in feature mean  $\delta$ . As shown in Figure 1c and Figure 1d, we observed (1) GCNs cannot separate the training data more accurately than MLP when shift is large (i.e., a larger  $\varepsilon_T$ ); (2) the performance gap  $\varepsilon_T - \varepsilon_S$  between the source and target is more pronounced in GCNs, confirming that **conditional shift of GNNs leads to a larger performance drop**. Having demonstrated that graph inductive bias often exacerbates conditional shift, our focus now turns to exploring potential mitigations of such shift during GNN training.

## 4 Graph UDA by Minimizing Conditional Shift

In the previous section, we discussed the exacerbated conditional shift for GNNs and how they relate to the performance degradation. Now, we present our approach to mitigate this conditional shift, quantified using the Wasserstein distance, in order to achieve effective graph UDA.

We first introduce the formal definition of optimal transport used in Eq. (3). Wasserstein distance can be computed as the optimal transport (OT) cost [29] between two distributions. Let  $\mathbf{d}(u_i, v_j)$  be the distance between two sets of samples  $\{u_i\}_{i=1}^m$  and  $\{v_j\}_{j=1}^m$  drawn from  $\mu_S$  and  $\mu_T$  respectively. OT solves the following problem:

$$\gamma^* = \arg \min_{\gamma \in \Gamma(\mu_s, \mu_t)} \sum_{i,j} \mathbf{d}(u_i, v_j) \gamma(i, j) \quad (8)$$

Specifically,  $\Gamma$  is the set of transportation plans that satisfy  $\Gamma(\mu_s, \mu_t) = \{\gamma \in \mathbb{R}_+^{m \times m} | \gamma \mathbb{1}_m = \gamma^\top \mathbb{1}_m = \mathbb{1}_m\}$ .

To estimate the empirical conditional shift, we calculate the Wasserstein distance between source label  $\mathbf{y}^s$  and estimated target label  $\hat{\mathbf{y}}^t = f(g(\mathbf{x}^t))$  as  $\widehat{\mathbf{W}}_1(\mu_S^f, \mu_T^f)$ . Hereby we introduce the learning problem of unsupervised graph domain adaptation by minimizing conditional shift. Given source labeled data  $\{(x_i^s, y_i^s)\}_{i=1}^N$  in  $\mathcal{G}^s$  and unlabeled target data  $\{x_j^t\}_{j=1}^N$  in  $\mathcal{G}^t$ , we optimize the following loss function,

$$\mathcal{L}_{\mathbf{GCONDA}} = \frac{1}{N} \sum_i \mathcal{L}_{\text{CE}}(y_i^s, \hat{y}_i^s) + \lambda \widehat{\mathbf{W}}_1(\mu_S^f, \mu_T^f), \quad (9)$$

$$\widehat{\mathbf{W}}_1(\mu_S^f, \mu_T^f) = \sum_{ij} \gamma_{ij}^* \cdot \mathbf{d}(y_i^s, \hat{y}_j^t), \mathbf{d}(\cdot) = \mathcal{L}_{\text{CE}}(\cdot) \quad (10)$$

where  $\hat{y}_i$  and  $\hat{y}_j$  are predictions on the source and target data produced by the classifier  $f$  and GNN encoder  $g$ .  $\mathcal{L}_{\text{CE}}$  is the cross-entropy loss. The loss consists of (1) classification loss on  $\mathcal{G}^s$ ; (2) estimated conditional shift  $\widehat{\mathbf{W}}_1$  between source and target samples in the batch;  $\Gamma^* \in \mathbb{R}^{N \times N}$  is the optimal transportation plan between node  $i$  in source graph  $\mathcal{G}^s$  and  $j$  in target  $\mathcal{G}^t$ ,  $\sum_{ij} \gamma_{ij}^* = 1$ .

Besides matching the conditional distribution  $\mathbf{P}(\mathbf{y}|\mathbf{h})$ , we propose to also mitigate the discrepancy marginal probability  $\mathbf{P}(\mathbf{h})$  following ideas from non-GNN UDA works [12] and call this variant **GCONDA++**. We define the distance between source data  $(h_i^s, y_i^s)$  and target data  $(h_j^t, \hat{y}_j^t)$  as,

$$\mathbf{d}((h_i^s, y_i^s), (h_j^t, \hat{y}_j^t)) = \alpha \|h_i^s - h_j^t\|^2 + \beta \mathcal{L}_{\text{CE}}(y_i^s, \hat{y}_j^t) \quad (11)$$

where  $h_i = g(x_i)$  is the output of a GNN. **GCONDA++** optimizes *both* the conditional and marginal distribution, that is,  $\widehat{\mathbf{W}}_1(\mu_S^{f \circ g}, \mu_T^{f \circ g})$ . If we set  $\beta = 0$ , our approach is equivalent to a DIRM method using optimal transport. In our experiments (*i.e.*, Table 1), we confirm this by showing that **GCONDA** with  $\beta = 0$  yields similar results to DIRM baselines.

**Generalization Bound of GCONDA.** Next we show the relationship between the estimated conditional shift and the generalization error under distribution shifts. We achieve this by extending theoretical results from [12].

**Theorem 4.1.** *Suppose  $\mathcal{F}$  is the hypothesis space of GNNs,  $\forall f \in \mathcal{F}$ ,*

$$\varepsilon_T(f) \leq \varepsilon_S(f) + \mathbf{W}_1(\mu_S^f, \mu_T^f) + \lambda^* + K_{\mathcal{L}} K_g \phi(c), \quad (12)$$

where  $\lambda^*$  is the joint optimal error,  $K_{\mathcal{L}}$  is the Lipschitz constant loss function of loss function  $\mathcal{L}$ ,  $K_g$  is the Lipschitz constant of GNN  $g$  and  $\phi(c)$  is the probabilistic Lipschitzness [6].

*Proof.* See Appendix §A.2. Assuming a model can generalize well on source and target data (*i.e.* small  $\lambda^*$ ), one can estimate the expected target error through OT cost  $\widehat{\mathbf{W}}_1$  and the Lipschitz constant  $K_g$  of the GNN function. Furthermore, if practitioners aim to improve the generalization on target domain, they can either (1) employ an UDA algorithm (*e.g.* **GCONDA**) to minimize  $\widehat{\mathbf{W}}_1$  or (2) change the GNN architecture to the one with a smaller  $K_g$  Lipschitz constant suggested by recent studies [11, 40].

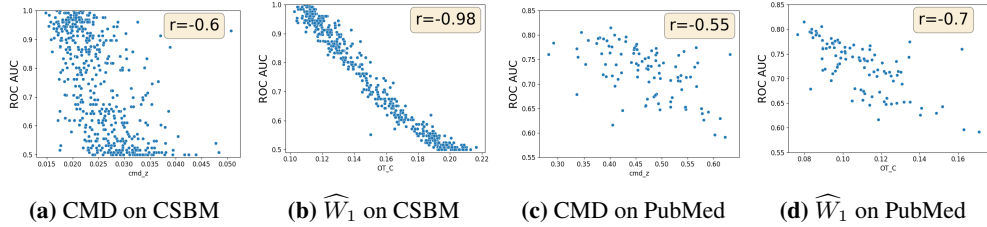


**Figure 2:** Comparison of CMD and transportation cost  $\widehat{W}_1$  (ours) for the same GCN model, x-axis the metric value and y-axis is the test ROC AUC. Each point in the plot corresponds to a pair of source and target graph. The Person correlation coefficient  $r$  (the larger abs values, the better) is shown on the top-right corner.

Note that the transportation cost term  $\widehat{W}_1$  in our loss function  $\mathcal{L}_{\text{GCONDA}}$  is an empirical estimation of  $\mathbf{W}_1(\mu_S^f, \mu_T^f)$  in the bound. To examine that whether the transportation cost is a good domain adaptation metric, we train a 2-layer graph convolution networks on  $\mathcal{G}_S$  and compute  $\widehat{W}_1$  on  $\mathcal{G}_T$ . The results are presented in Figure 2. Compared with CMD,  $\widehat{W}_1$  demonstrates a more clear correlation between discrepancy and testing performance on both synthetic graphs (*i.e.* CSBM) and real graphs (*i.e.* PubMed) when distribution shifts are present.

**Optimization.** We first fix the parameters of GNN  $g$  and classifier  $f$  to solve the transportation plan  $\Gamma^*$  using an EMD solver [8]. Then, we update the parameters of  $\{f, g\}$  through back-propagation of  $\mathcal{L}_{\text{GCONDA}}$ . It is also possible to update our parameters end-to-end with a neural optimal transport solver [22]. We perform scalable neighborhood sampling on the graph  $\mathcal{G}$  to obtain source and target subgraph samples for the input of the GNN  $g$ . Specifically, we adopt a sub-graph based sampling method - GraphSAINT [42] to obtain batch of nodes from source and target  $\mathcal{G}_b^s \sim \mathcal{G}_S, \mathcal{G}_b^t \sim \mathcal{G}_S$ , respectively. Refer to Appendix §B.1 for the **GCONDA** algorithm outline.

**Complexity.** In each step, let  $N$  be the size of mini-batch and  $d$  be the dimension size of hidden representation  $h_i \in \mathbb{R}^d$  and  $L$  classes, the additional computation cost of our method in each epoch is due to computing the transportation cost matrix  $C \in \mathbb{R}^{N \times N}$  and solving the optimal transportation  $\gamma^*$ . The cost matrix takes  $\mathcal{O}(N^2(d+L))$  time and the EMD solver takes  $\mathcal{O}(N^2)$  to solve the optimal transportation plan. Therefore, the total time complexity of **GCONDA** is  $\mathcal{O}(N^2 + N^2(d+L))$ . Due to the space limit, we conduct experiments on hyperparameter sensitivity and complexity study in Appendix §C.4.

## 5 Synthetic Experiments

In this section, we empirically validate our theoretical insights regarding the generalization ability and transferability of graph neural networks. We aim to answer the following questions: (a) "How do DURL methods perform under distribution shift on graphs?" and (b) "Does **GCONDA** provide any advantages over DURL for GNNs?"

We do this using two different families of synthetic graphs: (1) CSBM graphs, specifically `syn-csbm-pq` and `syn-csbm- $\delta$` , which involve synthetic conditional shifts in both the features and structure. Each sample in the CSBM graph consists of a training and testing graph, where the testing graph demonstrates either a feature shift  $\delta$  or a structure shift `pq`. (2) synthetic graphs constructed from real datasets, namely `syn-cora` and `syn-products`, with varying homophily ratios as described in previous work [45]. Detailed numerical results for all of the figures and the graph statistics can be found in Appendix §C.1. In this section, we compare our method **GCONDA** with well-known DURL algorithms including CMD [41] and CDAN [25] using graph convolution networks [19].

First, we compare two DURL algorithms - CDAN and CMD with **GCONDA** on two synthetic CSBM datasets. We tune the hyperparameters of all three algorithms using validation data obtained from the training graph. As illustrated in Figure 3a and Figure 3b, **GCONDA** outperforms both baselines in the presence of feature and structure distribution shifts. Notably, when the tested graph exhibits increased heterophily (small  $p/q$ ) or significant feature shifts (large  $\delta$ ), the performance of GNNs is more adversely affected. When distribution shifts are small, CMD enjoys similar to our method

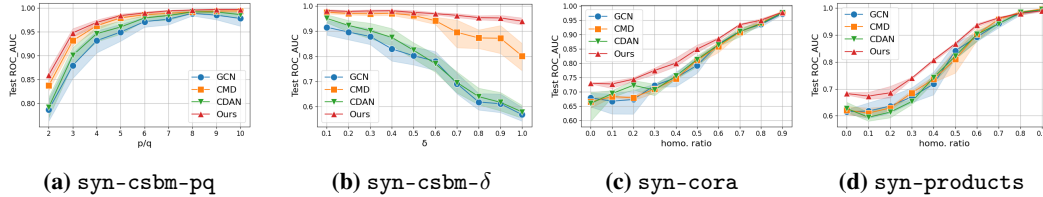


**Figure 3:** Domain adaptation results on synthetic graphs.

performance, confirming that DIRL methods work well with minor conditional shift. However, the difference between two methods becomes significant when testing distribution exhibits large conditional shift. We attribute the sub-optimal performance of DIRL to the fact that it solely optimizes the distribution discrepancy on  $\mathbf{P}(\mathbf{h})$  while neglecting the significant conditional shift.

In our second synthetic experiments, we examine the effectiveness of **GCONDA** on non-CSBM graphs. To do this, we follow the literature [45] studying GNNs in the low homophily setting, where *syn-cora* and *syn-products* are constructed from existing benchmarks via preferential attachment [2]. We train all the compared methods on the same "easy" graph, which has a homophily ratio of 1.0, for both datasets. Subsequently, we tested the models on target graphs with varying homophily ratios, ranging from 0.0 to 0.9. Based on our theoretical results, a target graph with a low homophily ratio is expected to result in a larger conditional shift. As depicted in Figure 3c and Figure 3d, we observe that the performance of the base GCN aligns with our expectations. **GCONDA** still mitigate the distribution shift better than DIRL methods.

## 6 Real Data Experiments

For real-world graphs, we will compare **GCONDA** with domain adaptation algorithms designed for neural networks and graph neural networks in both supervised and semi-supervised learning settings.

**Baselines.** In addition to the domain adaptation algorithms used in previous sections, we consider the following methods for comprehensive study under distribution shift: (1) MMD [24] and (2) DANN [14]. For graph-specific methods, we choose three representative methods: (1) UDAGCN [34] couples domain adversarial learning with graph attention mechanism; (2) SRGNN-IW [46] proposes to use instance weighting technique on GNN output embeddings; (3) Graph-EERM [35] proposes to augment training graph for invariance principles in risk minimization. As for our own ablations, we report the performance of DIRL version of our model ( $\beta = 0$  in in Eq. (11)) besides two variants of our methods **GCONDA** and **GCONDA ++**. All models are trained a single Nvidia A6000 GPU. Configurations of different algorithms on each dataset can be found in Appendix §B.2

**Table 1:** Semi-supervised classification on three different citation networks with OOD training samples. Results from the original paper [46] are marked  $\dagger$ . We mark the **best** and the second best results.

Method	Cora			Citeseer			PubMed		
	Micro-F1	Macro-F1	$\Delta$ Acc	Micro-F1	Macro-F1	$\Delta$ Acc	Micro-F1	Macro-F1	$\Delta$ Acc
IID training	80.8 $\pm$ 1.5	80.1 $\pm$ 1.3	0	70.2 $\pm$ 1.9	66.8 $\pm$ 1.7	0	79.7 $\pm$ 1.4	78.8 $\pm$ 1.4	0
OOD training	71.3 $\pm$ 4.1	69.2 $\pm$ 3.4	9.5	63.4 $\pm$ 1.8	61.2 $\pm$ 1.6	6.9	63.4 $\pm$ 4.2	58.7 $\pm$ 7.0	16.4
MMD	71.5 $\pm$ 4.9	69.5 $\pm$ 4.6	9.3	64.4 $\pm$ 1.2	62.0 $\pm$ 1.1	5.9	66.3 $\pm$ 4.2	63.5 $\pm$ 5.9	13.4
CMD $\dagger$	<u>72.1 <math>\pm</math> 4.4</u>	69.8 $\pm$ 3.7	8.7	63.9 $\pm$ 0.7	61.8 $\pm$ 0.6	6.4	69.4 $\pm$ 3.4	67.6 $\pm$ 4.0	10.4
DANN	71.5 $\pm$ 5.0	69.5 $\pm$ 4.6	9.3	64.7 $\pm$ 1.2	62.3 $\pm$ 1.1	5.6	64.5 $\pm$ 4.9	60.6 $\pm$ 7.8	15.2
CDAN	71.5 $\pm$ 5.1	69.5 $\pm$ 4.7	9.3	64.6 $\pm$ 1.3	62.2 $\pm$ 1.2	5.6	64.1 $\pm$ 5.0	59.9 $\pm$ 7.9	15.6
UDAGCN	36.2 $\pm$ 4.5	35.4 $\pm$ 4.3	44.6	33.8 $\pm$ 5.1	31.5 $\pm$ 7.7	36.4	40.6 $\pm$ 6.8	34.9 $\pm$ 6.8	39.1
EERM	68.3 $\pm$ 4.3	66.2 $\pm$ 3.9	12.5	62.3 $\pm$ 1.0	59.5 $\pm$ 1.0	7.9	61.6 $\pm$ 4.8	56.8 $\pm$ 7.7	18.1
SRGNN-IW $\dagger$	72.0 $\pm$ 3.2	69.5 $\pm$ 3.7	8.8	<b>66.1 <math>\pm</math> 0.9</b>	<u>63.4 <math>\pm</math> 0.9</u>	4.2	66.4 $\pm$ 4.0	64.0 $\pm$ 5.5	13.4
<b>GCONDA-DIRL</b>	71.7 $\pm$ 4.7	69.7 $\pm$ 4.3	9.1	64.6 $\pm$ 1.1	62.2 $\pm$ 1.0	5.6	68.3 $\pm$ 3.9	66.5 $\pm$ 4.7	11.4
<b>GCONDA</b>	71.7 $\pm$ 4.7	<u>70.2 <math>\pm</math> 2.7</u>	9.1	65.3 $\pm$ 0.8	63.3 $\pm$ 0.8	4.9	<u>71.5 <math>\pm</math> 2.9</u>	<u>70.4 <math>\pm</math> 3.1</u>	8.2
<b>GCONDA ++</b>	<b>72.6 <math>\pm</math> 3.1</b>	<b>70.7 <math>\pm</math> 3.0</b>	8.2	<u>65.6 <math>\pm</math> 0.9</u>	<b>63.5 <math>\pm</math> 0.9</b>	4.6	<b>73.0 <math>\pm</math> 2.5</b>	<b>71.9 <math>\pm</math> 2.5</b>	6.7

## 6.1 Semi-supervised Node Classification

GNNs are widely recognized for their effectiveness in node classification tasks, particularly when dealing with a limited amount of labeled data. In semi-supervised classification, source data is a small number of training nodes and target data are all of the remaining nodes in the same graph. Recently, SRGNN [46] found biased training data in semi-supervised learning can cause dramatic accuracy loss; they provide the algorithm to generate biased training nodes (referred to as OOD training in Table 1) on three semi-supervised learning benchmarks: Cora, Citeseer and PubMed [30]. We choose the best-performing GNN architecture from their paper - APPNP [20] and report the Micro-F1, and Macro-F1 for each method and the accuracy loss compared with IID training data. We are able to reproduce the performance gap between IID and OOD training data ( $\Delta$  in in Table 1). We begin by noting that most of the general domain adaptation algorithms such as CMD, MMD, and DANN can help improve the performance because conditional shift is small in this setting. Among these algorithms, we find that directly optimizing discrepancy metrics seems to be more effective and robust (smaller average loss and deviation over 100 runs) than adversarial methods (CDAN and DANN) which often require more tuning. Across the three datasets, **GCONDA ++** consistently achieves top-2 performance, while **GCONDA** (*i.e.*, only optimizing conditional shift) generally ranks second best. In addition, **GCONDA-DIRL** demonstrates similar performance to DIRL methods such as CMD and MMD. These observations suggest that the primary improvements stem from minimizing the estimated conditional shift  $\widehat{W}_1(\mu_S^f, \mu_T^f)$ .

**Table 2:** Domain adaptation on node and graph classification. We mark the **best** and the second best accuracy.

Method	Node Classification (Micro-F1)				Graph Classification (AUC)			
	ACM-DBLP <sub>small</sub>	ACM <sub>time</sub>	ACM-DBLP <sub>large</sub>	Avg. $\Delta$	BACE	BBBP	Clintox	Avg. $\Delta$
Base model	68.1 $\pm$ 2.1	78.8 $\pm$ 1.0	81.1 $\pm$ 0.2		64.8 $\pm$ 2.8	71.0 $\pm$ 8.7	52.8 $\pm$ 3.3	
CMD <sup>†</sup>	<u>75.5 <math>\pm</math> 4.4</u>	79.4 $\pm$ 0.7	75.2 $\pm$ 0.8	+0.97	60.4 $\pm$ 1.4	72.0 $\pm$ 1.8	55.0 $\pm$ 5.0	-0.40
DANN	70.1 $\pm$ 1.8	79.6 $\pm$ 0.4	81.6 $\pm$ 0.4	+1.10	67.4 $\pm$ 2.9	<u>74.0 <math>\pm</math> 2.3</u>	<u>61.6 <math>\pm</math> 3.6</u>	<u>+4.80</u>
CDAN	75.3 $\pm$ 4.3	79.3 $\pm$ 1.3	82.1 $\pm$ 0.3	<u>+2.90</u>	<b>69.1 <math>\pm</math> 1.8</b>	73.5 $\pm$ 1.7	57.5 $\pm$ 2.4	+3.83
UDAGCN	66.4 $\pm$ 5.1	79.3 $\pm$ 0.5	78.3 $\pm$ 2.6	-1.33	<u>67.9 <math>\pm</math> 1.4</u>	73.3 $\pm$ 2.1	60.7 $\pm$ 4.8	+ 4.43
EERM	64.9 $\pm$ 3.5	77.3 $\pm$ 0.4	81.0 $\pm$ 0.4	-1.60	N/A	N/A	N/A	N/A
SRGNN-IW	69.2 $\pm$ 1.6	79.5 $\pm$ 1.1	81.4 $\pm$ 0.4	0.70	65.2 $\pm$ 3.3	71.7 $\pm$ 2.8	57.3 $\pm$ 3.6	+1.87
<b>GCONDA-DIRL</b>	71.6 $\pm$ 2.3	<u>80.2 <math>\pm</math> 0.4</u>	<u>82.3 <math>\pm</math> 0.4</u>	+2.03	65.4 $\pm$ 2.4	69.3 $\pm$ 4.0	57.9 $\pm$ 3.6	+1.33
<b>GCONDA</b>	74.0 $\pm$ 4.7	80.1 $\pm$ 0.5	82.1 $\pm$ 0.3	+2.73	64.7 $\pm$ 2.0	70.0 $\pm$ 4.2	57.2 $\pm$ 2.1	+1.10
<b>GCONDA ++</b>	<b>78.5 <math>\pm</math> 4.0</b>	<b>80.3 <math>\pm</math> 0.8</b>	<b>82.5 <math>\pm</math> 0.3</b>	<b>+4.43</b>	67.8 $\pm$ 2.5	<b>74.4 <math>\pm</math> 3.0</b>	<b>61.7 <math>\pm</math> 2.4</b>	<b>+4.83</b>

## 6.2 Supervised Node and Graph Classification

In a fully-supervised setting, transfer learning is commonly employed to transfer knowledge across different domains for graph-structured data. This involves training a model on source graphs and inferring on target graphs. We conduct domain adaptation experiments on citation networks [32] and molecular graphs [18] for two tasks. The first task involves node classification by introducing domain shift between ACM and DBLP graphs, as well as time shift within the ACM graphs. The second task focuses on graph classification with scaffold shift, where the training and testing molecular graphs have different scaffold patterns. For node classification and graph classification, we adopt a 2-layer GCN [19] and a 5-layer GraphSAGE [17], respectively, following established practices. Specifically, for graph classification, we employ mean pooling to obtain the graph representations.

In Table 2, we make several key observations: (1) different algorithms exhibit varying performance under different settings, primarily due to the presence of various types of distribution shift; (2) on node classification, **GCONDA** and its variants usually outperforms the other baselines with a clear margin. This can be attributed to the fact that our approach has been theoretically designed to excel in node classification scenarios; (3) Domain adaptation algorithms, such as DANN, that are originally designed for neural networks exhibit better performance in graph classification tasks, because the graph classification task shares closer similarities with the image domain. Nevertheless, it is noteworthy that **GCONDA ++** consistently achieved top-3 rankings across all tasks and highest average improvement (*i.e.* Avg.  $\Delta$ ), indicating our potential usage on graph property predictions. For further details on the dataset and complementary experiments, please refer to Appendix §C.

## 7 Conclusion

In this work we establish the first theoretical connection between the inductive bias of GNNs and distribution shift by quantifying conditional shift. Our novel theoretical results show that conditional shift is often exacerbated by GNNs, explaining the limited performance of popular DRL methods on graph data. To remedy this shift in the latent space, we present a graph domain adaptation framework based on our theoretical results. Using a number different experiments on both synthetic and real data , we demonstrate that our method **GCONDA** results in a robust improvement on different kinds of domain shifts. As for future work, we have two notable directions to explore: (1) extend our analysis to other types of graph neural networks (2) develop more advanced GNNs following our theoretical results for graph domain adaptation.

## References

- [1] Martin Arjovsky, Léon Bottou, Ishaan Gulrajani, and David Lopez-Paz. Invariant risk minimization. *arXiv preprint arXiv:1907.02893*, 2019.
- [2] Albert-László Barabási and Réka Albert. Emergence of scaling in random networks. *science*, 286(5439):509–512, 1999.
- [3] Aseem Baranwal, Kimon Fountoulakis, and Aukosh Jagannath. Graph convolution for semi-supervised classification: Improved linear separability and out-of-distribution generalization. *arXiv preprint arXiv:2102.06966*, 2021.
- [4] Aseem Baranwal, Kimon Fountoulakis, and Aukosh Jagannath. Effects of graph convolutions in deep networks. *arXiv preprint arXiv:2204.09297*, 2022.
- [5] Shai Ben-David, John Blitzer, Koby Crammer, Alex Kulesza, Fernando Pereira, and Jennifer Wortman Vaughan. A theory of learning from different domains. *Mach. Learn.*, 79(1–2), 2010.
- [6] Shai Ben-David and Ruth Urner. Domain adaptation—can quantity compensate for quality? *Annals of Mathematics and Artificial Intelligence*, 70(3):185–202, 2014.
- [7] Beatrice Bevilacqua, Yangze Zhou, and Bruno Ribeiro. Size-invariant graph representations for graph classification extrapolations. In *International Conference on Machine Learning*, pages 837–851. PMLR, 2021.
- [8] Nicolas Bonneel, Michiel Van De Panne, Sylvain Paris, and Wolfgang Heidrich. Displacement interpolation using lagrangian mass transport. In *Proceedings of the 2011 SIGGRAPH Asia conference*, pages 1–12, 2011.
- [9] Ruichu Cai, Fengzhu Wu, Zijian Li, Pengfei Wei, Lingling Yi, and Kun Zhang. Graph domain adaptation: A generative view. *arXiv preprint arXiv:2106.07482*, 2021.
- [10] Ines Chami, Sami Abu-El-Haija, Bryan Perozzi, Christopher Ré, and Kevin Murphy. Machine learning on graphs: A model and comprehensive taxonomy. *Journal of Machine Learning Research*, 23(89):1–64, 2022.
- [11] Ching-Yao Chuang and Stefanie Jegelka. Tree mover’s distance: Bridging graph metrics and stability of graph neural networks. *arXiv preprint arXiv:2210.01906*, 2022.
- [12] Nicolas Courty, Rémi Flamary, Amaury Habrard, and Alain Rakotomamonjy. Joint distribution optimal transportation for domain adaptation. *Advances in Neural Information Processing Systems*, 30, 2017.
- [13] Yash Deshpande, Subhabrata Sen, Andrea Montanari, and Elchanan Mossel. Contextual stochastic block models. *Advances in Neural Information Processing Systems*, 31, 2018.
- [14] Yaroslav Ganin, Evgeniya Ustinova, Hana Ajakan, Pascal Germain, Hugo Larochelle, Francois Laviolette, Mario Marchand, and Victor Lempitsky. Domain-adversarial training of neural networks. *The journal of machine learning research*, 2016.
- [15] Arthur Gretton, Karsten M Borgwardt, Malte J Rasch, Bernhard Schölkopf, and Alexander Smola. A kernel two-sample test. *The Journal of Machine Learning Research*, 13(1):723–773, 2012.
- [16] Shurui Gui, Xiner Li, Limei Wang, and Shuiwang Ji. Good: A graph out-of-distribution benchmark. *arXiv preprint arXiv:2206.08452*, 2022.
- [17] Will Hamilton, Zhitao Ying, and Jure Leskovec. Inductive representation learning on large graphs. In *Advances in Neural Information Processing Systems*, pages 1024–1034, 2017.
- [18] Weihua Hu, Matthias Fey, Marinka Zitnik, Yuxiao Dong, Hongyu Ren, Bowen Liu, Michele Catasta, and Jure Leskovec. Open graph benchmark: Datasets for machine learning on graphs. *Advances in neural information processing systems*, 33:22118–22133, 2020.
- [19] Thomas N Kipf and Max Welling. Semi-supervised classification with graph convolutional networks. In *International Conference on Learning Representations*, 2017.
- [20] Johannes Klicpera, Aleksandar Bojchevski, and Stephan Günnemann. Predict then propagate: Graph neural networks meet personalized pagerank. *arXiv preprint arXiv:1810.05997*, 2018.

- [21] Pang Wei Koh, Shiori Sagawa, Henrik Marklund, Sang Michael Xie, Marvin Zhang, Akshay Balsubramani, Weihua Hu, Michihiro Yasunaga, Richard Lanus Phillips, Irena Gao, et al. Wilds: A benchmark of in-the-wild distribution shifts. In *International Conference on Machine Learning*, pages 5637–5664. PMLR, 2021.
- [22] Alexander Korotin, Lingxiao Li, Aude Genevay, Justin M Solomon, Alexander Filippov, and Evgeny Burnaev. Do neural optimal transport solvers work? a continuous wasserstein-2 benchmark. *Advances in Neural Information Processing Systems*, 34:14593–14605, 2021.
- [23] Trung Le, Tuan Nguyen, Nhat Ho, Hung Bui, and Dinh Phung. Lamda: Label matching deep domain adaptation. In *International Conference on Machine Learning*, pages 6043–6054. PMLR, 2021.
- [24] Mingsheng Long, Yue Cao, Jianmin Wang, and Michael Jordan. Learning transferable features with deep adaptation networks. In *International conference on machine learning*, pages 97–105. PMLR, 2015.
- [25] Mingsheng Long, Zhangjie Cao, Jianmin Wang, and Michael I Jordan. Conditional adversarial domain adaptation. *Advances in neural information processing systems*, 31, 2018.
- [26] Jiaqi Ma, Junwei Deng, and Qiaozhu Mei. Subgroup generalization and fairness of graph neural networks. *Advances in Neural Information Processing Systems*, 34, 2021.
- [27] Yao Ma, Xiaorui Liu, Neil Shah, and Jiliang Tang. Is homophily a necessity for graph neural networks? *arXiv preprint arXiv:2106.06134*, 2021.
- [28] David Mendez, Anna Gaulton, A. Patrícia Bento, Jon Chambers, Marleen De Veij, Eloy Felix, María P. Magariños, Juan F. Mosquera, Prudence Mutowo-Meullenet, Michal Nowotka, María Gordillo-Marañón, Fiona M. I. Hunter, Laura Junco, Grace Mugumbate, Milagros Rodríguez-López, Francis Atkinson, Nicolas Bosc, Chris J. Radoux, Aldo Segura-Cabrera, Anne Hersey, and Andrew R. Leach. ChEMBL: towards direct deposition of bioassay data. *Nucleic Acids Res.*, 47(Database-Issue):D930–D940, 2019.
- [29] Gaspard Monge. Mémoire sur la théorie des déblais et des remblais. *Mem. Math. Phys. Acad. Royale Sci.*, pages 666–704, 1781.
- [30] Prithviraj Sen, Galileo Namata, Mustafa Bilgic, Lise Getoor, Brian Galligher, and Tina Eliassi-Rad. Collective classification in network data. *AI magazine*, 29(3):93–93, 2008.
- [31] Jian Shen, Yanru Qu, Weinan Zhang, and Yong Yu. Wasserstein distance guided representation learning for domain adaptation. In *Proceedings of the AAAI Conference on Artificial Intelligence*, volume 32, 2018.
- [32] Jie Tang, Jing Zhang, Limin Yao, Juanzi Li, Li Zhang, and Zhong Su. Arnetminer: extraction and mining of academic social networks. In *Proceedings of the 14th ACM SIGKDD international conference on Knowledge discovery and data mining*, pages 990–998, 2008.
- [33] Petar Velickovic, Guillem Cucurull, Arantxa Casanova, Adriana Romero, Pietro Lio, and Yoshua Bengio. Graph attention networks. *arXiv preprint arXiv:1710.10903*, 2017.
- [34] Man Wu, Shirui Pan, Chuan Zhou, Xiaojun Chang, and Xingquan Zhu. Unsupervised domain adaptive graph convolutional networks. In *Proceedings of The Web Conference 2020*, 2020.
- [35] Qitian Wu, Hengrui Zhang, Junchi Yan, and David Wipf. Handling distribution shifts on graphs: An invariance perspective. *arXiv preprint arXiv:2202.02466*, 2022.
- [36] Keyulu Xu, Weihua Hu, Jure Leskovec, and Stefanie Jegelka. How powerful are graph neural networks? In *7th International Conference on Learning Representations, ICLR 2019, New Orleans, LA, USA, May 6-9, 2019*. OpenReview.net, 2019.
- [37] Nianzu Yang, Kaipeng Zeng, Qitian Wu, Xiaosong Jia, and Junchi Yan. Learning substructure invariance for out-of-distribution molecular representations. In *Advances in Neural Information Processing Systems*, 2022.
- [38] Nianzu Yang, Kaipeng Zeng, Qitian Wu, Xiaosong Jia, and Junchi Yan. Learning substructure invariance for out-of-distribution molecular representations. In *NeurIPS*, 2022.
- [39] Gilad Yehudai, Ethan Fetaya, Eli Meir, Gal Chechik, and Haggai Maron. From local structures to size generalization in graph neural networks. In *International Conference on Machine Learning*, pages 11975–11986. PMLR, 2021.

- [40] Yuning You, Tianlong Chen, Zhangyang Wang, and Yang Shen. Graph domain adaptation via theory-grounded spectral regularization. In *The Eleventh International Conference on Learning Representations*, 2023.
- [41] Werner Zellinger, Thomas Grubinger, Edwin Lughofer, Thomas Natschläger, and Susanne Saminger-Platz. Central moment discrepancy (cmd) for domain-invariant representation learning. *arXiv preprint arXiv:1702.08811*, 2017.
- [42] Hanqing Zeng, Hongkuan Zhou, Ajitesh Srivastava, Rajgopal Kannan, and Viktor Prasanna. Graphsaint: Graph sampling based inductive learning method. *arXiv preprint arXiv:1907.04931*, 2019.
- [43] Yizhou Zhang, Guojie Song, Lun Du, Shuwen Yang, and Yilun Jin. Dane: Domain adaptive network embedding. *arXiv preprint arXiv:1906.00684*, 2019.
- [44] Han Zhao, Remi Tachet Des Combes, Kun Zhang, and Geoffrey Gordon. On learning invariant representations for domain adaptation. In *International Conference on Machine Learning*, pages 7523–7532. PMLR, 2019.
- [45] Jiong Zhu, Yujun Yan, Lingxiao Zhao, Mark Heimann, Leman Akoglu, and Danai Koutra. Beyond homophily in graph neural networks: Current limitations and effective designs. *arXiv preprint arXiv:2006.11468*, 2020.
- [46] Qi Zhu, Natalia Ponomareva, Jiawei Han, and Bryan Perozzi. Shift-robust gnns: Overcoming the limitations of localized graph training data. *Advances in Neural Information Processing Systems*, 34, 2021.
- [47] Qi Zhu, Carl Yang, Yidan Xu, Haonan Wang, Chao Zhang, and Jiawei Han. Transfer learning of graph neural networks with ego-graph information maximization. In *NeurIPS*, 2021.

## Appendix

<b>A Theory details</b>	<b>15</b>
A.1 Proof of Theorem 3.1 . . . . .	15
A.2 Proof of Theorem 4.1 . . . . .	18
A.3 Additional discussion on DIRM . . . . .	19
<b>B Model Details</b>	<b>20</b>
B.1 GCONDA Algorithm . . . . .	20
B.2 Implementations . . . . .	20
B.3 Baseline Hyperparameters . . . . .	20
<b>C Experiment Details</b>	<b>21</b>
C.1 Dataset Details . . . . .	21
C.2 Complementary Results on Synthetic Domain Adaptation . . . . .	22
C.3 Complementary Results on Supervised Node Classification . . . . .	23
C.4 Hyperparameter and Complexity Study . . . . .	23
C.5 Additional Experiments on GraphOOD Benchmark . . . . .	24

## A Theory details

### A.1 Proof of Theorem 3.1

In Definition 3.3, we made several simplifications on original CSBM model to investigate its OOD generalization *w.r.t.* structure and feature distribution shifts. The original CSBM( $\mu, \nu, p, q$ ) is defined to have two different class means  $\mu$  and  $\nu$ . Given training and testing graphs as  $\mathcal{G}_S \sim \text{CSBM}(\mu, \nu, p, q)$  and  $\mathcal{G}_T \sim \text{CSBM}(\mu', \nu', p', q')$ , we let  $\nu = -\mu$  in CSBM by making  $\vec{0}$  the middle point of original feature mean of two classes. Without loss of generality, we let two graphs have same amount of nodes  $n = n'$  and edge density  $D = D'$ . Here we restate the pseudo conditional shifts  $\Delta_{\mathbf{y}|\mathbf{x}}$  on the hypothesis function used in Theorem 3.1. In this context, the function  $d$  is defined as an indicator function, which serves as a realization of Definition 3.2.

$$\Delta_{\mathbf{y}|\mathbf{x}} = \mathbb{E}_{\mathbf{x} \sim \mathbf{P}_t(\mathbf{x})} \left( \mathbb{I} \left[ \arg \max_y \mathbf{P}_s(\mathbf{y}|\mathbf{x}) \neq \arg \max_y \mathbf{P}_t(\mathbf{y}|\mathbf{x}) \right] \right), \quad (13)$$

**Theorem A.1** (Conditional Shift in GNNs). *Let the source graph  $\mathcal{G}_S = \text{CSBM}(\mu, p, q)$ , and a target graph  $\mathcal{G}_T = \text{CSBM}(\mu', p', q')$ , where  $D$  and  $D'$  represent their average degrees respectively. Additionally, let  $\Phi(\cdot)$  denote the cumulative distribution function (CDF) of a multivariate Gaussian distribution defined by distance. Then the introduced distribution shift between  $\mathcal{G}_S$  and  $\mathcal{G}_T$  can be quantified via the estimated conditional shift of  $\mathbf{x}$  and  $\mathbf{h}$  as:*

$$\Delta_{\mathbf{y}|\mathbf{x}} = \frac{\Phi((1+\delta)\|\mu\|) - \Phi((1-\delta)\|\mu\|)}{2}, \Delta_{\mathbf{y}|\mathbf{h}} = \frac{\Phi(\|\mu'_{h,-1}\|) - \Phi(\|\mu'_{h,1}\|)}{2}, \quad (14)$$

where  $\mu'_{h,1} = \sqrt{D'} \frac{p'-q'}{p'+q'} \mu - \sqrt{D'} \delta \mu$  and  $\mu'_{h,-1} = \sqrt{D'} \frac{q'-p'}{p'+q'} \mu - \sqrt{D'} \delta \mu$ .

**Proposition 1.** *Through training with hinge loss, the linear classifier  $f$  on original feature  $\mathbf{x}$  and GNN latent space  $\mathbf{h}$  have the same optimal hyperplane  $\mathcal{P} = \{\mathbf{x} | \mathbf{w}^T \mathbf{x} + b = 0\}$  characterized by  $\mathbf{f}(\mathbf{w}^*, b^*)$ ,  $\mathbf{w}^* = \mu$  and  $b^* = 0$ .*

*Proof.* On a CSBM graph  $\mathcal{G}(\mu, p, q)$ , the data distribution on feature  $\mathbf{x}$  is,

$$\begin{aligned} x_i &\sim \mathcal{N}(\mu, \mathbf{I}), y_i = 1, \\ x_i &\sim \mathcal{N}(-\mu, \mathbf{I}), y_i = -1 \end{aligned} \quad (15)$$

Since  $\mathbf{x}$  is a standard Gaussian, the output of the  $\arg \max$  operator is identical to the optimal  $\mathbf{f}^*(x)$ . Furthermore, the distributions on the source and target share the same support. Thus, the indicator function in Equation 13 can be simplified as the expected difference in predictions between the optimal source classifier  $\mathbf{f}$  and the optimal target classifier  $\mathbf{f}'$  on the target data, that is,

$$\Delta_{\mathbf{y}|\mathbf{x}} = \mathbb{E}_{\mathbf{x} \sim \mathbf{P}_t(\mathbf{x})} (\mathbb{I} [\mathbf{f}(x) \neq \mathbf{f}'(x)]), \quad (16)$$

We first discuss the conditional shift on the feature  $\mathbf{x}$  of the target graphs. Since we assume that the distribution shift on the feature  $\mu$  is controlled by  $\delta$ , the centers of the two classes on the target graphs are located at  $-(1+\delta)\mu$  and  $(1-\delta)\mu$ :

$$\begin{aligned} x'_i &\sim \mathcal{N}((1-\delta)\mu, \mathbf{I}), y_i = 1, \\ x'_i &\sim \mathcal{N}(-(1+\delta)\mu, \mathbf{I}), y_i = -1, \end{aligned} \quad (17)$$

The optimal classifier is  $\mathbf{f}(\mu, 0)$  on source graph and  $\mathbf{f}'(\mu, \delta\mu)$  on target CSBM graph. We further partition the computation of  $\Delta_{\mathbf{y}|\mathbf{x}}$  on two classes, that is  $\Delta_{\mathbf{y}=1|\mathbf{x}} + \Delta_{\mathbf{y}=-1|\mathbf{x}}$ . When  $y'_i = 1$ , the different predictions (*i.e.*  $f(x_i) \neq f'(x_i)$ ) are those samples between 0 and  $-\delta\mu$  in 1-dimension case. Considering the probability density function  $\mathbf{P}_t(\mathbf{x})$  in Equation 17,  $\Delta_{\mathbf{y}=1|\mathbf{x}}$  is calculated as,

$$\Delta_{\mathbf{y}=1|\mathbf{x}} = \frac{1}{\sqrt{2\pi}} \int_{-\delta\mu}^0 \exp\left\{-\frac{(t - (1-\delta)\mu)^2}{2}\right\} dt \quad (18)$$

The CDF of the standard Gaussian distribution is denoted by the  $\Phi$  function.

$$\Phi(x) = \frac{1}{\sqrt{2\pi}} \int_{-\infty}^x \exp\left\{-\frac{t^2}{2}\right\} dt \quad (19)$$

In standard multivariate ( $d > 1$ ) Gaussian distribution, we define the CDF as a monotonic function regarding the distance to the Gaussian mean  $\Phi(\|\cdot\|)$ .

To represent the conditional shift use  $\Phi$ , we flip the axis  $x = -x$  and translate the distribution into a standard Gaussian  $\mathcal{N}(0, \mathbf{I})$  by moving  $1 - \delta\mu$  as described in Figure 4.

$$\Delta_{y=1|x} = \Phi(\|\mu\|) - \Phi(\|\mu - \delta\mu\|), \quad (20)$$

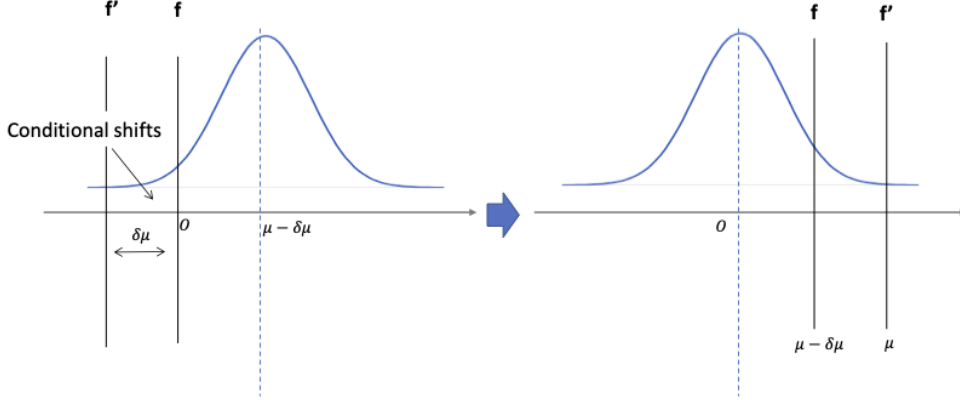


**Figure 4:** Representing  $\Delta_{y=1|x}$  with  $\Phi$

Similarly, for class  $y_i = -1$ , we can have,

$$\Delta_{y=-1|x} = \Phi(\|\mu + \delta\mu\|) - \Phi(\|\mu\|), \quad (21)$$

Since we have the same amount of nodes for each class, we get the value of conditional shifts on original features and weighted average of two classes,

$$\Delta_{y|x} = \frac{\Delta_{y=-1|x} + \Delta_{y=1|x}}{2} = \frac{\Phi(\|\mu + \delta\mu\|) - \Phi(\|\mu - \delta\mu\|)}{2} = \frac{\Phi((1 + \delta)\|\mu\|) - \Phi((1 - \delta)\|\mu\|)}{2}, \quad (22)$$

Now, we are ready to discuss the conditional shift on the GCN transformed features  $\mathbf{h}$ . Now, we are ready to discuss the conditional shift on GCN transformed features  $\mathbf{h}$ . The feature of a node in a CSBM graph that has been transformed using GCN is obtained as a weighted mean of  $D$  (average degree) distinct Gaussian random variables. Among these variables,  $\frac{p}{p+q}$  constitute the intra-class variables, while  $\frac{q}{p+q}$  make up the inter-class variables. As a result, the data distribution on  $\mathbf{h}$  is as follows:

$$\begin{aligned} h_i &\sim \mathcal{N}\left(\frac{p-q}{p+q}\mu, \frac{1}{\sqrt{D}}\mathbf{I}\right), y_i = 1, \\ h_i &\sim \mathcal{N}\left(\frac{q-p}{p+q}\mu, \frac{1}{\sqrt{D}}\mathbf{I}\right), y_i = -1 \end{aligned} \quad (23)$$

We rescale the Gaussian distribution output by graph convolution to standard Gaussian distribution,

$$h_i \sim \mathcal{N}\left(\sqrt{D} \cdot \frac{p-q}{p+q}\mu, \mathbf{I}\right), \text{ for } y_i = 1.$$

Consequently, on target graph,

$$\begin{aligned} h'_i &\sim \mathcal{N}\left(\sqrt{D'} \cdot \frac{p'(1-\delta)\mu - q'(1+\delta)\mu'}{p' + q'}, \mathbf{I}\right), y_i = 1, \\ h'_i &\sim \mathcal{N}\left(\sqrt{D'} \cdot \frac{q'(1-\delta)\mu - p'(1+\delta)\mu'}{p' + q'}, \mathbf{I}\right), y_i = -1 \end{aligned} \quad (24)$$

Let  $\mu'_{h,1} = \sqrt{D'} \frac{p'-q'}{p'+q'} \mu - \sqrt{D'} \delta \mu$  and  $\mu'_{h,-1} = \sqrt{D'} \frac{q'-p'}{p'+q'} \mu - \sqrt{D'} \delta \mu$ , we are ready to finish the proof by calculation conditional shifts on target data.

$$\Delta_{\mathbf{y}|\mathbf{h}} = \frac{1}{2} \left( \Phi\left(\frac{\mu'_{h,-1}{}^\top \mu_h}{\|\mu\|}\right) - \Phi\left(\frac{\mu'_{h,1}{}^\top \mu_h}{\|\mu_h\|}\right) \right) = \frac{\Phi(\|\mu'_{h,-1}\|) - \Phi(\|\mu'_{h,1}\|)}{2}. \quad (25)$$

□

Now let's discuss the relative conditional shift on  $\mathbf{x}$  and  $\mathbf{h}$  when structure or feature deviates from training, respectively.

**Corollary A.1.1** (GNNs exacerbate Conditional Shift). *Assuming only homophily ratio changes  $p/q \neq p'/q'$ , the conditional shift is always exacerbated by the 1-layer GCN since  $\Delta_{\mathbf{y}|\mathbf{x}} = 0$ . When there is only a feature shift  $\delta\mu$ , the shift will be amplified by the GCN as  $\sqrt{D'}\delta\mu$ , potentially leading to larger conditional shifts.*

*Proof.* When graph structure  $(p', q')$  changes on target graph while  $\mu$  remains the same (i.e.  $\delta = 0$ ),  $\Delta_{\mathbf{y}|\mathbf{h}} \geq \Delta_{\mathbf{y}|\mathbf{x}} = 0$

When there is a distribution shift in the feature mean of the class ( $\delta > 0$ ), we define  $\mu' = \sqrt{D'} \frac{p'-q'}{p'+q'} \mu$  and obtain the following expression:

$$\Delta_{\mathbf{x}|\mathbf{h}} = \frac{\Phi(\|\mu + \delta\mu\|) - \Phi(\|\mu - \delta\mu\|)}{2}, \Delta_{\mathbf{y}|\mathbf{h}} = \frac{\Phi(\|\mu' + \sqrt{D'}\delta\mu\|) - \Phi(\|\mu' - \sqrt{D'}\delta\mu\|)}{2}. \quad (26)$$

Although obtaining a closed-form solution for when GCNs exacerbate conditional shift, i.e.,  $\Delta_{\mathbf{x}|\mathbf{h}} < \Delta_{\mathbf{y}|\mathbf{h}}$ , is complicated, we can analyze the effect of varying  $\delta$  on  $\mathbf{x}$  and  $\mathbf{h}$ . We observe that both  $\Delta_{\mathbf{x}|\mathbf{h}}$  and  $\Delta_{\mathbf{y}|\mathbf{h}}$  are monotonically increasing functions of  $\delta$ . In the latent space  $\mathbf{h}$  w.r.t.  $\mu'$ , the magnitude of feature shift is amplified by  $\sqrt{D'}$ .

□

**Corollary A.1.2** (Relation between conditional shift and generalization). *Conditional shift upper bounds the performance gap between source and target, i.e.  $\Delta > |\varepsilon_{\mathcal{T}} - \varepsilon_{\mathcal{S}}|$ . The expected target error  $\varepsilon_{\mathcal{T}}$  for linear classifiers  $f$  and GNNs  $f \circ g$  are,*

$$\varepsilon_{\mathcal{T}}(f) = 1 - \frac{\Phi((1+\delta)\|\mu\|) + \Phi((1-\delta)\|\mu\|)}{2}, \varepsilon_{\mathcal{T}}(f \circ g) = 1 - \frac{\Phi(\|\mu'_{h,-1}\|) + \Phi(\|\mu'_{h,1}\|)}{2}. \quad (27)$$

*Proof.* We begin by computing the expected target error  $\varepsilon_{\mathcal{T}}$  on  $\mathbf{x}$ , denoted as  $\varepsilon_{\mathcal{T}}(f)$ . Unlike the calculation of conditional shift, the expected error is evaluated on the target graph  $\mathcal{G}_{\mathcal{T}}$  and can be expressed as follows:

$$\varepsilon_{\mathcal{T}}(f) = \mathbb{E}_{\mathbf{x} \sim \mathcal{P}_t(\mathbf{x})} (\mathbb{I}[\mathbf{f}(x) \neq y]), \quad (28)$$

We recall that the feature means of the two classes are  $(-(1+\delta)\mu, (1-\delta)\mu)$ . For class 1, the optimal  $f$  fails to classify  $x_i$  correctly if  $w^T x_i + b < 0$ , with a distance of  $|(1-\delta)\mu|$  or more from  $(1-\delta)\mu$ . The probability of such instances can be calculated as  $1 - \Phi(|(1-\delta)\mu|)$ . Combining this with class  $-1$ , we obtain the following result:

$$\varepsilon_{\mathcal{T}}(f) = \underbrace{\frac{1 - \Phi(\|\mu + \delta\mu\|)}{2}}_{\text{error of class -1}} + \underbrace{\frac{1 - \Phi(\|\mu - \delta\mu\|)}{2}}_{\text{error of class 1}} \quad (29)$$

Similarly, on a source graph, the expected error is  $\varepsilon_{\mathcal{S}}(f) = 1 - \Phi(\|\mu\|)$  and  $\Phi(\cdot)$  is a monotonically increasing function. Therefore, we have  $|\varepsilon_{\mathcal{S}} - \varepsilon_{\mathcal{T}}| = \Phi(\|\mu\|) - \frac{\Phi(\|\mu + \delta\mu\|) + \Phi(\|\mu - \delta\mu\|)}{2}$ . Furthermore, we can calculate  $\Delta_{\mathbf{y}|\mathbf{x}} - |\varepsilon_{\mathcal{S}} - \varepsilon_{\mathcal{T}}|$  as follows:

$$\Delta_{\mathbf{y}|\mathbf{x}} - |\varepsilon_{\mathcal{S}} - \varepsilon_{\mathcal{T}}| = \Phi(\|\mu + \delta\mu\|) - \Phi(\|\mu\|) > 0 \quad (30)$$

Regarding graph convolution networks, the class centroids after GCN are  $\mu'_{h,1}$  and  $\mu'_{h,-1}$  as calculated in Theorem 3.1. The expected error of a linear classifier  $f$  on the output of GCN  $g$  is obtained as follows:

$$\varepsilon_{\mathcal{T}}(f \circ g) = 1 - \frac{\Phi(\|\mu'_{h,-1}\|) + \Phi(\|\mu'_{h,1}\|)}{2} \quad (31)$$

We re-use the definition of  $\mu'$  from the proof of Corollary 3.1.1. We can now complete the proof:

$$\Delta_{\mathbf{h}|\mathbf{x}} - |\varepsilon_{\mathcal{S}} - \varepsilon_{\mathcal{T}}| = \Phi(\|\mu' + \sqrt{D'}\delta\mu\|) - \Phi(\|\mu'\|) > 0 \quad (32)$$

□

## A.2 Proof of Theorem 4.1

**Theorem A.2.** *Suppose  $\mathcal{F}$  is the hypothesis space of GNNs,  $\forall f \in \mathcal{F}$ ,*

$$\varepsilon_{\mathcal{T}}(f) \leq \varepsilon_{\mathcal{S}}(f) + \mathbf{W}_1(\mu_{\mathcal{S}}^f, \mu_{\mathcal{T}}^f) + \lambda^* + K_{\mathcal{L}}K_g\phi(c), \quad (33)$$

where  $\lambda^*$  is the joint optimal error;  $K_{\mathcal{L}}$  is the Lipschitz constant loss function of  $\mathcal{L}$ ,  $K_g$  is the Lipschitz constant of GNN  $g$  and  $\phi(c)$  is the probabilistic Lipschitzness [6].

*Proof.* Following the approach in [12], we introduce  $f^*$  as the optimal labeling function in the hypothesis space  $\mathcal{F}$ , giving us:

$$\begin{aligned} \varepsilon_{\mathcal{T}}(f) &= \mathbb{E}_{(\mathbf{x}, \mathbf{y}) \sim \mathbf{P}_t} \mathcal{L}(\mathbf{y}, f(\mathbf{x})) \\ &\leq \mathbb{E}_{(\mathbf{x}, \mathbf{y}) \sim \mathbf{P}_t} \mathcal{L}(\mathbf{y}, f^*(\mathbf{x})) + \mathcal{L}(f(\mathbf{x}), f^*(\mathbf{x})) \\ &= \mathbb{E}_{(\mathbf{x}, \mathbf{y}) \sim \mathbf{P}_t} \mathcal{L}(f(\mathbf{x}), f^*(\mathbf{x})) + \varepsilon_{\mathcal{T}}(f^*) \\ &= \mathbb{E}_{(\mathbf{x}, f(\mathbf{x})) \sim \mathbf{P}_t^f} \mathcal{L}(f(\mathbf{x}), f^*(\mathbf{x})) + \varepsilon_{\mathcal{T}}(f^*) \\ &= \varepsilon_{\mathcal{T}}(f^*) - \varepsilon_{\mathcal{S}}(f^*) + \varepsilon_{\mathcal{S}}(f^*) + \varepsilon_{\mathcal{T}}(f^*) \\ &\leq |\varepsilon_{\mathcal{T}}^f(f^*) - \varepsilon_{\mathcal{S}}(f^*)| + \underbrace{\varepsilon_{\mathcal{S}}(f^*) + \varepsilon_{\mathcal{T}}(f^*)}_{\lambda^*} \end{aligned} \quad (34)$$

Now we introduce the definition of  $K_g$  and  $\phi(c)$  in the theorem. The Lipschitz constant of GNNs has garnered considerable attention in recent studies [11]. In our analysis, we view the data distribution as rooted subtrees [47] centered around node  $i$ , denoted as  $x_i = T_i$ , where  $T_i$  are sampled from graph  $G$ . We define the Lipschitz constant  $K_g$  of GNNs as follows:

$$|f(T_i) - f(T_j)| \leq K_g |l(T_i) - l(T_j)| \leq K_g \quad (35)$$

where  $l : T_i \rightarrow [0, 1]^d$  is a bounded function maps node features in the rooted subtree to real values, e.g. mean aggregation and normalization in GraphSAGE [17].

**Definition A.1** (Probabilistic Transfer Lipschitzness [12]). *Let  $\phi : \mathbb{R} \rightarrow [0, 1]$ , a labeling function  $f : X \rightarrow \mathbb{R}$  and a joint distribution  $\Gamma$  over  $\mu_{\mathcal{S}}$  and  $\mu_{\mathcal{T}}$ , the  $\phi$ -transfer Lipschitzness represents for all  $c$ :*

$$\mathbf{P}_{(\mathbf{x}_s, \mathbf{x}_t)}[|f(\mathbf{x}_s) - f(\mathbf{x}_t)| > cd(\mathbf{x}_s, \mathbf{x}_t)] \leq \phi(c) \quad (36)$$

Let  $\mu_{\mathcal{S}}^f = \mathbf{P}_s(\mathbf{x}, \mathbf{y})$  and  $\mu_{\mathcal{T}}^f = \mathbf{P}_t^f(\mathbf{x}, f(\mathbf{x}))$  denote the source data distribution and the estimated target data distribution, respectively.  $\varepsilon_{\mathcal{T}}^f(f^*)$  can be interpreted as the discrepancy in predictions

between  $f$  and  $f^*$ . Given  $\Gamma^*$  is the optimal transportation plan of **GCONDA**, we have:

$$\begin{aligned}
& |\varepsilon_{\mathcal{T}}^f(f^*) - \varepsilon_{\mathcal{S}}(f^*)| \\
&= \left| \int \mathcal{L}(y, f^*(\mathbf{x})) \mathbf{d}(\mathbf{P}_t^f - \mathbf{P}_s) \right| \\
&= \left| \int (\mathcal{L}(f(\mathbf{x}_t), f^*(\mathbf{x}_t)) - \mathcal{L}(y_s, f^*(\mathbf{x}_s))) \mathbf{d}\Gamma^*((\mathbf{x}_s, \mathbf{y}_s), (\mathbf{x}_t, f(\mathbf{x}_t))) \right| \\
&\leq \int \left| (\mathcal{L}(f(\mathbf{x}_t), f^*(\mathbf{x}_t)) - \mathcal{L}(y_s, f^*(\mathbf{x}_s))) \right| \mathbf{d}\Gamma^*((\mathbf{x}_s, \mathbf{y}_s), (\mathbf{x}_t, f(\mathbf{x}_t))) \\
&\leq \int \left| \mathcal{L}(f(\mathbf{x}_t), f^*(\mathbf{x}_t)) - \mathcal{L}(f(\mathbf{x}_t), f^*(\mathbf{x}_s)) \right| + \left| \mathcal{L}(f(\mathbf{x}_t), f^*(\mathbf{x}_s)) - \mathcal{L}(y_s, f^*(\mathbf{x}_s)) \right| \mathbf{d}\Gamma^*((\mathbf{x}_s, \mathbf{y}_s), (\mathbf{x}_t, f(\mathbf{x}_t))) \\
&\leq \int K_{\mathcal{L}} \left| f^*(\mathbf{x}_s) - f^*(\mathbf{x}_t) \right| + \mathcal{L}(f(\mathbf{x}_t), \mathbf{y}_s) \mathbf{d}\Gamma^*((\mathbf{x}_s, \mathbf{y}_s), (\mathbf{x}_t, f(\mathbf{x}_t))) \tag{37} \\
&\leq \int c * K_{\mathcal{L}} d(\mathbf{x}_s, \mathbf{x}_t) + \mathcal{L}(y_s, f(\mathbf{x}_t)) \mathbf{d}\Gamma^*((\mathbf{x}_s, \mathbf{y}_s), (\mathbf{x}_t, f(\mathbf{x}_t))) + K_{\mathcal{L}} K_g \phi(c) \tag{38} \\
&\leq \mathbf{W}_1(\mu_{\mathcal{S}}^f, \mu_{\mathcal{T}}^f) + K_{\mathcal{L}} K_g \phi(c) \tag{39}
\end{aligned}$$

Line (25) is a consequence of Lipschitz constant and triangle inequality on  $\mathcal{L}$ . Line (26) applies  $\phi(c)$ -transfer lipschitzness on  $f^*(\mathbf{x})$ . The last line (27) is achieved by setting  $\alpha = c * K_{\mathcal{L}}$  in Eq. (11) of the main paper. We complete the proof by combining Eq. (34) and Eq. (27).  $\square$

### A.3 Additional discussion on DIRL

In Section 3.1 of the main paper, we introduced the covariate shift assumption on DIRL, which alternatively assumes a small conditional shift. However, even with this assumption, our synthetic experiment in Section 5 shows that the best DIRL method (*i.e.* CMD) still yield unsatisfactory results. To further illustrate this from a theoretical perspective, we restate an existing study on the conditional shift in DIRL.

**Theorem A.3** (Limits of learning invariant representations under conditional shift). [44] *Suppose markov chain  $X \xrightarrow{\mathbf{g}} Z \xrightarrow{h} \hat{Y}$  and  $d_{\text{JS}}$  is the Jensen-Shannon distance,*

$$\varepsilon_{\mathcal{S}}(h \circ \mathbf{g}) + \varepsilon_{\mathcal{T}}(h \circ \mathbf{g}) \geq \frac{1}{2} (d_{\text{JS}}(\mathcal{D}_{\mathcal{S}}^Y, \mathcal{D}_{\mathcal{T}}^Y) - d_{\text{JS}}(\mathcal{D}_{\mathcal{S}}^Z, \mathcal{D}_{\mathcal{T}}^Z)^2)$$

According to the above theorem, when  $\mathbf{P}(Y|X)$  is different on source and target, minimizing source risk and  $\mathcal{H}\Delta\mathcal{H}$ -divergence leads to a small JS distance  $d_{\text{JS}}(\mathcal{D}_{\mathcal{S}}^Z, \mathcal{D}_{\mathcal{T}}^Z)$ . As a consequence, the marginal label shift  $d_{\text{JS}}(\mathcal{D}_{\mathcal{S}}^Y, \mathcal{D}_{\mathcal{T}}^Y)$  dominating the the lower bound of joint source and target risk. If conditional shift is large, DIRL cannot achieve accurate predictions on target. In Figure 5, we train a domain adversarial neural network [14] and project the node TSNE embeddings of source and target CSBM graphs. Two different colors indicate class labels,  $\mathbf{O}$  dots are source data and  $\mathbf{X}$  are target samples. When the conditional shift is small and covariate shift assumption holds approximately, DANN can separate different classes well for both source and target domains (left). However, when there is large conditional shift, the classification accuracy on target is low because it only minimizes discrepancy between representations, and classes end up intermixed.

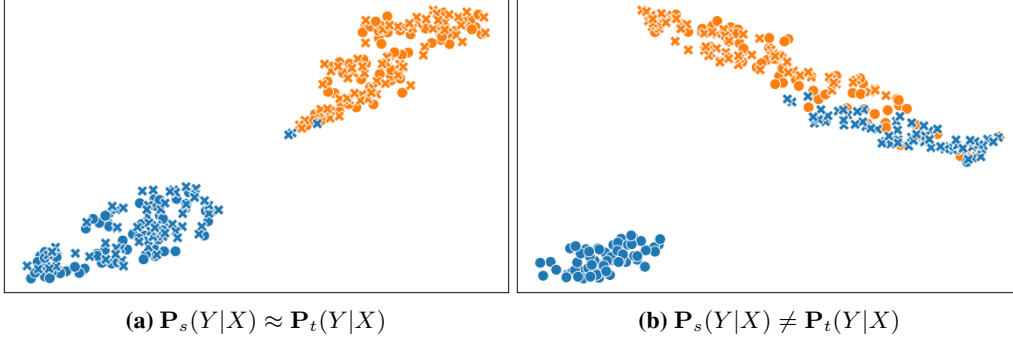


Figure 5: Performance of DIRL methods under small or large conditional shifts.

## B Model Details

### B.1 GCONDA Algorithm

---

**Algorithm 1:** Pseudo code for **GCONDA** optimization

---

- 1 **Input:** Training graph  $\mathcal{G}_S$ ; testing graph  $\mathcal{G}_T$ ;
  - 2 Graph Sampler **SAMPLE**;
  - 3 **Output:** GNNs  $g$  and classifier  $f$  with trained weights;
  - 4 **for** each batch of  $(\mathcal{G}_b^s, x_b^s, y_b^s)$  and  $(\mathcal{G}_b^t, x_b^t)$  from **SAMPLE** **do**
  - 5     fix  $f, g$ , compute  $\mathbf{d}(\cdot) \leftarrow$  Eq. (10) of the main paper
  - 6     solve  $\Gamma^*$  using an OT solver
  - 7     fix  $\Gamma^*$  and update the weights of  $f, g \leftarrow$  Eq. (9) of the main paper
  - 8 **end**
- 

In the algorithm, we use node classification with a neighborhood sampler as an example. For graph classification, each sample  $(\mathcal{G}_b, x_b, y_b)$  is a different graph sampled from source or target.

### B.2 Implementations

We implement our method and all other baselines using torch-geometric library. We list the graph neural network specifications used in our experiments,

1. Synthetic node classification - model architecture: Graph Convolutional Networks [19], hidden dimension: 16, activation: SiLU, number of layers: 2, dropout: 0.0
2. Semi-supervised node classification - model architecture: APPNP [20], hidden dimension: 32, number of layers: 2, dropout: 0.0,
3. Supervised node classification - model architecture: Graph Convolutional Networks [19], hidden dimension: 128, activation: ReLU, number of layers: 2, dropout: 0.2
4. Supervised graph classification - model architecture: GraphSAGE [17], hidden dimension: 300, activation: ReLU, number of layers: 5, dropout: 0.5

For supervised node classification, we utilized the RandomWalk GraphSAINT [42] sampler with a batch size of 256, step size of 50, and walk length of 2. We independently run experiments 10 times and report the mean and standard deviation in all table and figures. All models are trained on a single Nvidia A6000 GPU. The code for each experiment can be found in separate folder in supplementary materials.

### B.3 Baseline Hyperparameters

In our experiments, we employed the following baselines and performed hyperparameter tuning on the validation set. Specifically, each baseline has hyperparameters as follow,

1. For MMD,  $\alpha \in \{0.01, 0.1, 0.5, 1\}$  controls the weight of regularization.

**Table 3:** Dataset Statistics.

	syn-csbm	syn-cora	syn-products	cora	citeseer	pubmed	DBLP	ACM	BACE	BBBP	Clintonx
# Graphs	500	30	30	1	1	1	2	2	1513	2039	1478
# Nodes	128	1,490	10,000	2,708	3,327	19,717	78,509	23,343	34	24	26
# Edges	1,280	2,965	59,640	5,278	4,614	44,325	1,001,300	162,106	74	52	56
# Classes	2	5	10	7	6	3	5	5	2	2	2

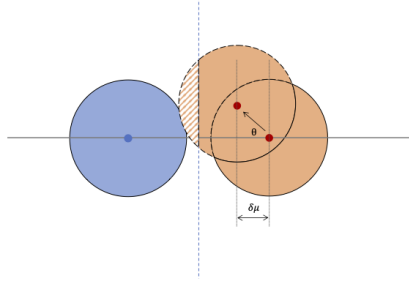


**Figure 6:** Illustration of creating feature shift on CSBM graphs.

- For CMD,  $k \in \{1, 3, 5, 7, 10\}$  determines the number of central moment.  $\alpha \in \{0.01, 0.1, 0.5, 1\}$  controls the weight of regularization.
- For DANN,  $\alpha$  is set in  $\{0.1, 0.5, 1\}$  for reverse gradients in backward pass.  $\beta \in \{0.01, 0.1, 0.5, 1\}$  controls the weight of regularization.
- For CDAN,  $\lambda$  is a hyper-parameter between source classifier and conditional domain discriminator.  $l_0 \in \{0.01, 0.1, 1\}$  and  $h_i \in \{0.1, 1, 2\}$  are the initial value and final value of  $\lambda$ .  $\beta \in \{0.01, 0.1, 0.5, 1\}$  controls the weight of regularization.
- For UDAGCN, the balance parameters  $\gamma_1$  and  $\gamma_2$  are adjusted carefully in the searching space  $\{0.1, 0.3, 0.5, 0.7, 1.0\}$ , respectively. The adaptation rate  $\lambda$  is the following schedule:  $\lambda = \min(\frac{2}{1+\exp(-10p)} - 1, 0.1)$ , and the  $p$  is changing from 0 to 1 within the training process as [34].
- For EERM, we search the best learning rate  $\alpha_f \in \{0.0001, 0.0002, 0.001, 0.005, 0.01\}$  for GNN backbone, the learning rate  $\alpha_g \in \{0.0001, 0.001, 0.005, 0.01\}$  for graph editors, the weight  $\beta \in \{0.2, 0.5, 1.0, 2.0, 3.0\}$  for combination, the number of edge editing for each node  $s \in \{1, 5, 10\}$ , the number of iterations  $T \in \{1, 5\}$  for inner update before one-step outer update.
- For SRGNN-IW<sup>†</sup>, the main hyper parameters in the sampler PPR-S are  $\alpha \in \{0.01, 0.1, 0.5, 1\}$ ,  $\gamma \in \{10, 50, 100, 200, 500\}$ . When the graph is large,  $\epsilon = 0.001$  is set in the local algorithm for sparse PPR approximation.  $\lambda \in \{0.1, 0.5, 1, 2\}$  is the penalty parameter for the discrepancy regularizer. The lower bound for the instance weight  $B_l$  is in  $\{0.1, 0.2, 0.5, 1.0\}$ .
- Hyperparameters of GCONDA  $\alpha$  and  $\beta$  are selected between  $\{0.01, 0.1, 1\}$ .

## C Experiment Details

### C.1 Dataset Details

In the main paper, we perform node classification and graph classification tasks on 11 different datasets with distribution shift. The statistics of these graphs are presented in Table 3. We will now discuss the selection criterion or creation process for each dataset in detail.

**CSBM Dataset Generation.** In our experiments, we set the feature size  $d$  and average degree  $D$  of CSBM graph in Definition 3.3 graph as 128 and 10, respectively.

For structure shift (*i.e.* syn-csbm-pq), each time we first sample a feature mean  $\mu \sim \mathcal{N}(0, \frac{1}{\sqrt{d}})$ , where  $d$  is the dimension of the feature. Then source graph is generated with a fixed  $p/q = 5$  while each target graph is generated under a random  $p/q$  between  $\{1, \dots, 10\}$ . Such that we ensure the

features of both graph are generated with the same Gaussian distribution and their homophily ratios are different.

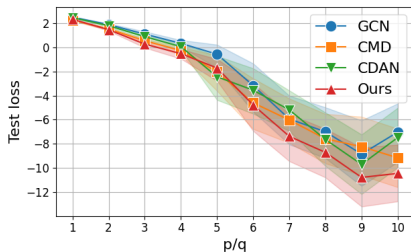
For feature shift (*i.e.*  $\text{syn-csbm-}\delta$ ), we generate  $\mu'$  by translating mean by  $\delta\mu$  and rotate  $\mu'$  by  $\theta$  (from 0 to 60 degrees). In corollary 3.1.2, we use the same  $\delta$  to describe the classification error. When  $\delta$  is small, feature shift is small and test feature mean  $\mu'$  is close to original feature mean. The rotation is added to avoid trivial adaptation like translation. Figure 6 illustrates the process of creating features shifts in our experiment. The dataset generation code can be found in uploaded code named `cSBM_gendata.py`.

**DBLP-ACM Dataset.** In the main paper, we conduct the transfer learning experiments with *domain shift* and *time shift* for node classification. These experiments use three sets of citation networks, which are constructed on the datasets provided by ArnetMiner [32]. Specifically, for domain shift, we adopt two sets of ACM-DBLP citation networks of different sizes. The small set namely  $\text{ACM-DBLP}_{\text{small}}$  is proposed by [34]. It includes the papers extracted from ACMv9 (between years 2000 and 2010) and DBLPv8 (after year 2010). The large set,  $\text{ACM-DBLP}_{\text{large}}$  is constructed on DBLPv12 (before 2017) and ACMv8 (before 2017). As to time shift, we utilize ACMv9 across different time periods, specifically, before or after 2010, to build two citation networks,  $\text{ACM}_{\text{time}}$ . In our experiments, we consider these datasets as undirected graphs and each edge representing a citation relation between two papers. The papers are classified to some of the predefined categories according to its research topics.  $\text{ACM-DBLP}_{\text{small}}$  has six categories including “Database”, “Data mining”, “Artificial intelligent”, “Computer vision”, “Information Security” and “High Performance Computing”. For  $\text{ACM-DBLP}_{\text{large}}$  and  $\text{ACM}_{\text{time}}$ , there are five categories including “Database”, “Data mining”, “Artificial intelligent”, “Computer vision”, and “Natural Language Processing”. We evaluate our proposed methods by conducting multi-label classification on these three sets of citation networks.

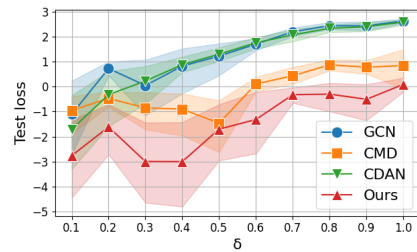
**Graph Classification Datasets.** There are 10 molecular property prediction datasets from Open Graph Benchmark [18]. These graphs are known to be affected by the scaffold split of the training and testing data. To compare different domain adaptation algorithms, we rank the performance degradation by comparing validation and test accuracy. From Table 2 in the main paper, we select the top-3 datasets with the highest degradation: BACE, BBBP, and Clintox. We choose these datasets because they exhibit the most pronounced “negative” distribution shifts.

## C.2 Complementary Results on Synthetic Domain Adaptation

In Figure 7, we provide the test logloss plot of our experiments on CSBM graphs as complimentary results of Figure 3 of the main paper, respectively. The test loss also correlates well with domain adaptation bound introduced in Theorem 4.1. When distribution shift becomes more significant, for example a smaller  $p/q$  or larger  $\delta$ , the target loss increases. In addition, we present the numerical results used to draw Figure 3a and 3b of the main paper in Table 4 and Table 5.



(a) Testing loss of different DA algorithms.



(b) Testing Loss of different DA algorithms.

**Figure 7:** Domain adaptation on datasets constructed from real graphs. We use homophily ratio 1.0 for training and plot the base GCN performance as well as domain adaption algorithms on three test graphs per interval.

**Table 4:** syn-csbm- $p/q$  (Fig. 3a). Mean ROC and standard deviation per method (with structure shift  $p/q$ ).

Method	syn-csbm- $p/q$									
	1	2	3	4	5	6	7	8	9	10
GCN	62.6 ± 6.3	78.7 ± 8.2	87.9 ± 8.8	93.1 ± 8.1	94.9 ± 5.7	97.1 ± 3.6	97.6 ± 4.4	98.8 ± 1.7	98.4 ± 3.0	97.8 ± 4.6
CMD	66.0 ± 5.0	83.7 ± 4.0	93.1 ± 3.3	96.2 ± 2.6	97.9 ± 1.5	98.5 ± 1.4	98.8 ± 1.4	99.1 ± 1.2	99.3 ± 0.9	99.3 ± 1.0
CDAN	62.7 ± 5.9	79.2 ± 8.1	90.0 ± 6.5	94.6 ± 5.4	96.0 ± 4.7	97.9 ± 2.0	98.4 ± 3.6	99.1 ± 1.1	99.1 ± 1.4	98.6 ± 2.7
Ours	68.1 ± 5.4	85.9 ± 4.0	94.7 ± 3.0	96.9 ± 2.1	98.4 ± 1.3	98.9 ± 1.0	99.4 ± 0.7	99.5 ± 0.5	99.7 ± 0.5	99.6 ± 0.5

**Table 5:** syn-csbm- $\delta$  (Fig. 3b). Mean ROC and standard deviation per method (with feature shift  $\delta$ ).

Method	syn-csbm- $\delta$									
	0.1	0.2	0.3	0.4	0.5	0.6	0.7	0.8	0.9	1.0
GCN	91.5 ± 10.7	89.6 ± 9.9	87.9 ± 11.2	82.9 ± 14.3	80.2 ± 13.8	78.1 ± 13.6	69.1 ± 12.8	61.8 ± 13.1	61.1 ± 13.4	56.8 ± 10.2
CMD	97.5 ± 1.9	97.0 ± 1.8	96.9 ± 2.6	97.1 ± 2.5	96.2 ± 5.1	94.2 ± 5.5	89.5 ± 18.5	87.3 ± 15.5	87.2 ± 19.2	80.1 ± 20.2
CDAN	93.5 ± 7.5	90.2 ± 9.3	87.1 ± 11.4	84.4 ± 12.6	79.0 ± 13.5	72.6 ± 12.4	66.6 ± 12.1	60.8 ± 13.0	59.4 ± 12.2	55.5 ± 8.0
Ours	98.1 ± 1.5	97.8 ± 1.5	98.0 ± 1.8	98.1 ± 1.5	97.4 ± 4.1	96.9 ± 1.8	96.3 ± 2.4	95.3 ± 3.3	95.2 ± 3.9	94.0 ± 5.4

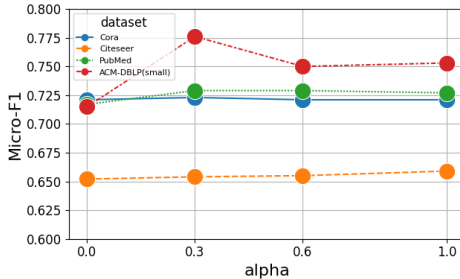
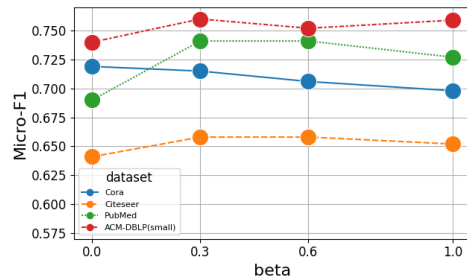
### C.3 Complementary Results on Supervised Node Classification

Due to the space limit, we only report the Micro-F1 in the Table 2 of the main paper. In Table 6, we include the results on both Micro-F1 and Macro-F1.

### C.4 Hyperparameter and Complexity Study

**Choices of  $\alpha$  and  $\beta$ .** The main difference between **GCONDA** and **GCONDA ++** is the introduction of aligning marginal distribution  $(\mu_S^g, \mu_T^g)$  together with conditional shift controlled by hyperparameter  $\alpha$  in Eq.(11) of the main paper. In this section we study how varying  $\alpha, \beta$  between  $[0, 1]$  in **GCONDA ++** affects the performance. We conduct 10 runs for each  $\alpha$  while fixing  $\beta = 0.1$  on four node classification datasets and vice versa. In Figure 8a, we observed that **GCONDA ++** does not consistently outperform **GCONDA** ( $\alpha = 0$ ) except dataset ACM-DBLP. Because different domains may have different word distributions as node features, and in this case we find that regularizing the representation shift appears to be helpful. In Figure 8b, we observe that the performance on all four datasets improves when  $\beta > 0$ , further validating that minimizing conditional shift is a key factor in our framework. Overall, our performance is not sensitive to the hyper parameters within a reasonable range.

**Time and Space Complexity of GCONDA.** We would like to provide further details on training time and extra costs on a non-citation graph from Open Graph Benchmark [18] - ogbn-proteins. In ogbn-proteins, nodes represent proteins, and edges indicate different types of biologically meaningful associations between proteins. The task is to predict the presence of protein functions in a multi-label binary classification setup, where there are 112 kinds of labels to predict in total. It is considered as reasonably large with 132 thousand nodes and 39 million edges. We report the actual running time and actual GPU usage per epoch varying batch size  $N$  in Table 7. We observe that the training time of **GCONDA** increases only slightly when the batch size is set to 128. The additional space complexity is negligible for all batch sizes. The additional time complexity, as explained earlier, is

**(a)** Node classification accuracy varying  $\alpha$ **(b)** Node classification accuracy varying  $\beta$

**Table 6:** Full result of supervised node classification. We report mean and standard deviation on Micro and Macro F1.

Method	ACM-DBLP <sub>small</sub>		ACM <sub>time</sub>		ACM-DBLP <sub>large</sub>	
	Micro-F1	Macro-F1	Micro-F1	Macro-F1	Micro-F1	Macro-F1
Base model	68.1 ± 2.1	68.2 ± 2.4	78.8 ± 1.0	76.1 ± 0.7	81.1 ± 0.2	79.1 ± 0.2
MMD	65.9 ± 2.2	65.3 ± 3.1	79.0 ± 1.0	76.1 ± 1.0	81.7 ± 0.3	79.6 ± 0.3
CMD <sup>†</sup>	75.5 ± 4.4	71.9 ± 6.8	79.4 ± 0.7	75.9 ± 0.7	75.2 ± 0.8	74.7 ± 0.7
DANN	70.1 ± 1.8	70.5 ± 1.7	79.6 ± 0.4	76.9 ± 0.4	81.6 ± 0.4	80.0 ± 0.4
CDAN	75.3 ± 4.3	75.2 ± 4.6	79.3 ± 1.3	76.4 ± 0.9	82.1 ± 0.3	80.0 ± 0.2
UDAGCN	66.4 ± 5.1	64.1 ± 6.2	79.3 ± 0.5	74.6 ± 0.4	78.3 ± 2.6	74.5 ± 2.7
EERM	64.9 ± 3.5	60.0 ± 3.2	77.3 ± 0.4	74.5 ± 0.3	81.0 ± 0.4	78.1 ± 0.4
SRGNN-IW <sup>†</sup>	69.2 ± 1.6	69.9 ± 1.7	79.5 ± 1.1	76.7 ± 0.8	81.4 ± 0.4	79.5 ± 0.3
<b>GCONDA</b> ( $\alpha = 0$ )	74.0 ± 4.7	73.3 ± 4.9	80.1 ± 0.5	77.2 ± 0.4	82.1 ± 0.3	80.0 ± 0.3
<b>GCONDA</b> ( $\beta = 0$ )	71.6 ± 2.3	71.2 ± 2.6	80.2 ± 0.4	77.3 ± 0.3	82.3 ± 0.4	80.2 ± 0.4
<b>GCONDA</b>	78.5 ± 4.0	78.1 ± 4.3	80.3 ± 0.8	77.3 ± 0.6	82.5 ± 0.3	80.4 ± 0.3

**Table 7:** Additional Time and Space Complexity of **GCONDA**.

Method	Time			Space		
	128	256	512	128	256	512
GraphSAGE	6min04s	6min20s	6min51s	5035MB	5075MB	5149MB
<b>GCONDA</b>	6min46s	8min42s	14min08s	5081MB	5129MB	5389MB

primarily influenced by the batch size. Choosing an appropriate batch size, such as 128 or 256, can reduce the computation cost of solving the optimal transportation plan in **GCONDA**.

### C.5 Additional Experiments on GraphOOD Benchmark

We performed additional experiments on graph classification using six datasets obtained from the data curators of DrugOOD [38]. The DrugOOD dataset is derived from the ChEMBL website, which houses a large-scale bioassay deposition [28]. The dataset offers various indicators for splitting, such as assay, scaffold, and size. Furthermore, we applied three different splitting schemes to both IC50 and EC50 categories in DrugOOD. As a result, we obtained six datasets: EC50- $\star$  and IC50- $\star$ , where the suffix  $\star$  denotes the specific splitting scheme (IC50/EC50-assay/scaffold/size). This approach enables us to comprehensively evaluate the performance of our method under different environmental definitions. All six datasets focus on ligand-based affinity prediction (LBAP), where each molecule is labeled as active or inactive. For all datasets, we followed the default training-validation-test split outlined following [38]. During training, we utilized all molecules in the training set to optimize the model parameters. Subsequently, we selected hyperparameters based on the validation set and reported the results on the test molecule set using the model that achieved the best performance on the validation set.

For graph classification, to build the base model, we adopt a 4-layer GIN [36] for node representations and a mean pooling layer for graph representations followed by a linear head to make prediction. The experimental results are presented in Table 8. Upon the careful observations, we can find several noteworthy discoveries. Firstly, it becomes evident that the performance of different algorithms varies significantly across different settings, predominantly due to the presence of distinct distribution shifts. This implies that algorithm selection should be tailored to the specific characteristics of the dataset and the nature of the distribution shift. In addition, our proposed approach (**GCONDA**) and its variants consistently outperform the other baseline methods. This persistent superiority can be attributed to the deliberate design of our approach, which prioritizes optimal performance in graph classification scenarios. The underlying techniques and mechanisms employed by our approach effectively leverage the inherent structure and relationships within graph nodes, leading to superior classification accuracy. Furthermore, the standout performance of our approach (**GCONDA ++**) should not be overlooked. Across all datasets, **GCONDA ++** consistently achieved a top ranking, showcasing its robustness and

**Table 8:** Experimental results for graph classification on Drugood datasets (including Accuracy and AUC scores).

Model	lbap_core_ec50					
	Assay		Scaffold		Size	
	ACC	AUC	ACC	AUC	ACC	AUC
Base Model	87.89	69.46	70.32	59.66	67.86	61.53
CMD	70.68	50.15	58.51	47.99	67.22	57.97
DANN	87.49	64.70	68.36	58.16	67.78	47.58
CDAN	87.54	69.25	70.88	60.23	68.14	61.10
UDAGCN	82.79	73.05	72.38	61.23	69.70	61.06
SRGNN-IW	87.39	74.04	72.05	60.35	68.94	60.33
<b>GCONDA</b>	88.62	<b>74.40</b>	71.94	60.45	69.42	59.94
<b>GCONDA ++</b>	<b>88.84</b>	71.22	<b>73.57</b>	<b>61.75</b>	<b>70.34</b>	<b>61.57</b>

Model	lbap_core_ic50					
	Assay		Scaffold		Size	
	ACC	AUC	ACC	AUC	ACC	AUC
Base model	81.21	68.34	74.04	63.69	72.80	61.51
CMD	74.24	68.55	72.54	60.33	68.30	58.14
DANN	83.22	70.08	76.00	66.37	70.08	63.45
CDAN	83.06	71.29	76.52	66.42	72.87	64.79
UDAGCN	81.34	69.89	74.66	63.77	72.96	64.79
SRGNN-IW	82.91	71.00	75.51	63.80	73.32	64.85
<b>GCONDA</b>	83.47	<b>72.40</b>	<b>77.77</b>	<b>67.50</b>	73.42	62.50
<b>GCONDA ++</b>	<b>83.56</b>	71.64	77.36	66.04	<b>73.92</b>	<b>65.87</b>

effectiveness. This consistent high performance across various datasets signifies the potential of our approach to accurately predict graph properties and opens up promising avenues for its practical applications.